1992

Characterization of old cast iron by ultrasound

Hernan P. Estupinan
Lehigh University

AUTHOR:

Estupinan, Hernan P.

TITLE:

Characterization of Old Cast Iron by Ultra-Soung

DATE: May 31, 1992

CHARACTERIZATION OF OLD CAST IRON BY ULTRASOUND

BY

HERNAN P. ESTUPINAN

A Thesis

Presented to the Graduate Committee

of Lehigh University

in Candidacy for the Degree of

Master in Science

in

Materials Science and Engineering

Lehigh University

1992

CERTIFICATE OF APPROVAL

This Thesis is accepted and approved in partial fulfillment of the requirements for the degree of Master of Science

May 12, 1992
(date)

Professor in Charge

Chairman of Department

ACKNOWLEDGEMENTS

The author express his sincere gratitude to Dr. John D. Wood for his guidance, assistance, and encouragement throughout the course of this project.

He would also like to thank to John Slanski, Daniel Henkel, and Rob Kowalik for their moral support during this time at Lehigh University.

Finally, many thanks to my family, Maria and Ivan, to my mother and brothers, for their support in this adventure.

TABLE OF CONTENTS

LIST OF TABLES

LIST OF FIGURES

1.- ABSTRACT

At the beginning of the 20th century the cast iron industry played a vital role in the country's industrial and economic development. In the early years of this century, many civil engineering projects were developed with the use of gray cast iron as a basic support of the structures such as the under river New York-New Jersey train tunnel. Little is known about the metallurgical conditions of the cast iron used, and the principal objective of this study was to characterize the actual metallurgical and mechanical condition of the castings.

For that objective, specimens were prepared from different castings that were tunnel liners. From these specimens, tensile, hardness, impact, metallographic, ultrasound and eddy current tests were performed.

Because of the access only from one side of the liners, the ultrasound technique with pulse-echo mode constitutes a suitable method for the evaluation. Results obtained with the use of low frequency transducers improves the back reflection signal, which in turn let you know the general condition of the casting and obtain an accurate idea of the mechanical properties of the castings.

A high ultrasound velocity for the cast iron testing is directly related with the high tensile strength. At high

ultrasound velocity corresponds a high tensile strength, and at low ultrasound velocity corresponds a low tensile strength. Then the ultrasound technique appears to be a useable technique for the evaluation of the actual conditions of the cast iron material used in old civil engineering structures.

2.- INTRODUCTION

The iron castings are so widely used in our highly mechanized society that iron foundries constitute the nation fifth largest manufacturing industry, with a yearly tonnage of more than a triple that all other ferrous and non ferrous castings combined, producing annually as much as 18 millon tons of product, with a value of nearly a 12 billion dollars.[1]

Engineers know cast iron is a cheap structural material. It has always been that,and with a metallurgical control, is an alloy that can be produced with high strength comparable with some steels and certain other desirable properties that only this alloy is capable of providing.[2] (A general discussion of the physical metallurgy of cast iron is presented in the Appendix 1). In 1642, Sangus Iron Works, in Lynn,Mass., was the first iron foundry established in America. At the end of the 19th century and the beginning of the 20th century, the cast iron industry was so big that it played a vital role in the country's industrial and economic development. In the early years of this century, many civil engineering projects were developed with the use of this material such as in the basic support of the structures as in the under river New York-New Jersey train tunnel, and almost one hundred years later, the structure continues working. The tunnel liners are made up cast iron segments having a width of 0.6 m (2 feet), a length of 1.6 m (5.5 feet), a heavy wall of 3.5 cm (1.375 inch), and each box-like casting is joined to

adjacent segments by bolts, as showed in the sketch of the Figure #1. The specifications to which the castings were produced do not indicate the chemical composition. The mechanical properties specified are a minimum tensile strength of 110 MPa (16 ksi). The additional test for the material is in a 2.54 cm (1 inch) square bar must support a drop of a 4.54 kg (10 pound) weight from a height of 30.48 cm (1 foot) onto the bar supported on a 30.48 cm (12 inch) centers.[3]

The metal working conditions at 1900, of course were different that in 1990, especially in the area of physical metallurgy and solidification of cast iron, but the basic principles of the casting process continue being the same. From the study of the literature from the early part of the 20th century it is possible observe that the principal difference has to do with the chemical composition of the cast iron. For example in the first two decades of the 20th century the differences include higher total carbon content, high phosphorous and sulphur percentages, and the addition of titanium in the castings, gave the final result of gray cast iron with a ferrite matrix as a basic constituent, and with a large size graphite flakes. In the study made by Saveur[3] it is possible observe that the high phosphorus content (up to 2.8 weight %) in the cast iron which was a normal practice at 20th century first two decades, as it could be noticed from the explanation given by Stead that "a relatively high proportion of phosphorus does not produce extreme brittleness in cast

iron".[3]

Little is known about the metallurgical conditions of the cast iron structure used in the tunnel liners in the under river tunnel, and the principal objective of this work was to study the real metallurgical structures and mechanical properties of the casting used.

For that purpose, samples were obtained from tunnel liners castings and these were used to obtain the data on the mechanical properties and metallurgical conditions of the material. Different tests were done such as tensile test, hardness, metallography, impact, ultrasound, and Eddy current.

Due to the conditions inside of the tunnel, much emphasis were placed on the use of nondestructive evaluation (NDE) procedures for the evaluation of the castings. Since the access to the castings in the tunnel is limited to only one side, the ultrasound technique was the principal NDE technique studied.

In addition, one of the main concerns of the evaluation was to know the physical condition of the inaccessible surface especially in relation with the decrease of wall thickness caused by corrosion processes. The ultrasound technique with pulse-echo mode constitutes a suitable method applicable to the case, and in fact the results obtained with the use of low frequency transducers let the inspector to know the general condition of the casting and to obtain an accurate idea of the mechanical properties of the casting in the range of study.

3.- BACKGROUND

The term cast iron is a generic one, referring to a family of materials differing widely in their properties. In general, a cast iron is a alloy of iron with carbon (up to 4.3 weight %), and silicon (up to about 3.5 weight %) which ordinarily is not usefully malleable as cast.[4]

The demand for iron castings is based in the nature of cast irons as engineering materials and their economic advantages. Cast irons offers a wide range of metallic properties such as strength, hardness, machinability, wear resistance, corrosion resistance, and other properties. Furthermore, the foundry properties of cast irons in terms of yield, fluidity, shrinkage, casting soundness, ease of production, make the material highly desirable for casting purposes.

The metallurgy of cast iron is more complex than its economics and, indeed, is one of the most complex metallurgical systems. The physical metallurgy of cast iron is summarized in the following paragraph and is discussed more completely in Appendix 1.

For the study of cast iron it is necessary consider the two diagrams: the stable diagram iron-graphite and the metastable iron-iron carbide diagram because the iron carbide or cementite is the metastable phase. The two diagrams are shown in Figure #2. Steels and white cast iron obey the

metastable diagram, whereas the cast iron obey both, the equilibrium iron-graphite and the metastable Fe-Fe_3C phase diagrams.

In cast iron, silicon is an important alloying element. The addition of silicon promotes the graphitization in gray iron decomposing the cementite in iron plus graphite. In the Figure # 2, it is possible to observe the increase of the eutectoid temperature as the silicon content increases and the displacement of the eutectoid composition to a lower carbon content.

Phosphorous is another important alloying element. The majority of gray iron contains between 0.1 and 0.9 % P. Phosphorous forms the micro-constituent steadite,which is a complex eutectic of iron and iron-phosphide (Fe-Fe3P)[1]. Steadite is relatively fragile and has the tendency to form a continuous network between the dendrites of austenite which decreases the cast iron toughness.

In the solidification process the kind of iron formed depends upon the composition, nucleating agents, and the solidification rate. Two phases must be considered in the growth of the solid, (I) the metallic phase and (II) the non-metallic phase[5].

The metallic phase which crystallizes from the melt is the austenite (gamma phase) and this phase grows at a rate determined by the solute diffusion in the liquid. On the other hand, graphite is a typically non-metallic phase, which

grows interconnected within the eutectic cell in a continuous skeleton of growing members in three dimensions, and also the growing graphite phase is apparently independent of the involved metallic (austenite) phase.[6]

The term eutectic cell is used in the field of cast iron solidification to show a structure of two interwoven crystals, in which all the graphite flakes are interconnected, as is the austenite.[7]

Finally, it is interesting to notice that the mechanical properties of cast iron depend on the microstructure, which is obtained as a consequence of the chemical composition and the solidification behavior.[8] Considering a cast iron with a constant matrix (pearlite to ferrite ratio), the tensile strength, hardness, and Young's modulus change with different graphite morphologies. In other words, the shape, size and distribution of the graphite, as well as the cell size, have a big effect on the mechanical properties of the cast iron.[9]

4.- EXPERIMENTAL PROCEDURE

For the experimental procedure samples were cut from different castings that were the tunnel liners, as shown in the Figure # 1. From these samples, specimens for the

different tests were prepared accordingly with the ASTM standards.[10,11,12]

4.1.- CHEMICAL COMPOSITION

The chemical analysis was done by optical emission spectroscopy for manganese,phosphorous, silicon, molybdenum, copper and nitrogen. For carbon and sulfur were used wet chemical analysis. In addition was required the carbon combined, in order to obtain the graphitic carbon. The chemical composition was done from coupons from each one of the castings as shown the Figure # 1.

4.2.- HARDNESS

Hardness is the most commonly determined property of metal because it is a simple test and many of the useful properties are related to it hardness. The Brinell hardness test is used for cast iron because the Brinell test impression is large enough to average the hardness of the constituents in the microstructure.

Rockwell B or C scale tests can be used on machined surfaces, but several tests should be made and averaged, discarding the extreme values because of inordinate influence by the graphite flakes[1].

The hardness scale used was the Brinell 3000 which was done with a constant load of 3000 Kg applied in a 10 mm ball penetrator. Different times of loading are recommended[1] and after the evaluation, 20 seconds was used as loading time. In the case that the size of the sample was too small for the

Brinell test, a Rockwell B (HRB) value was used as alternative.

4.3.- TENSILE TEST

Gray irons are commonly classified by their minimum tensile strength. A Class 20 indicates that it has a nominal tensile strength of 138 MPa (20 ksi). A Class designation may be used to indicate a grade of iron even when the tensile strength is not an important consideration. The ASTM A-48 has the Class 20 (20 Ksi) as the low tensile strength cast iron.[10]

To obtain the tensile strength, tensile coupons were machined from each one of the castings, both from the ribs and from the wall of the casting, and tensile standard bars were machined from each coupon accordingly with the standard ASTM E-8, and A-48.[10,11] The sketches in the Figure # 1 show the position of the tensile coupons.

4.4.- IMPACT TEST

The Charpy notched impact test was selected to evaluate the toughness of the castings. The material was prepared from each casting from longitudinal and transversal directions, being longitudinal the direction of the flow of the liquid metal during the casting process and the transversal the corresponding normal direction, as is showed in the sketch of the Figure # 4. The coupons were extracted from the same location in each casting and the final machined bars were done

from the middle of the transversal section of the piece. The Charpy specimen and associated test procedure provides a relatively severe test of material toughness. The number of engineering test that have been devised to evaluate the material toughness and the transition from brittle to ductile fracture in materials is almost a legion. One of these, however, stands out because of its simplicity, easy of preparation, economy, and almost universal acceptance - the Charpy impact test with a V-notched specimen. It can be seen that it consist of a bar with a square cross section 10 mm (0.39 in) on a side. A V-notch is cut across one of its faces. The specimen is supported on its two ends in a fashion of a simple beam. It is then impacted on the opposite side directly behind the notch with a knife edge mounted at the center of percussion of a heavy pendulum hammer, which is dropped from a fixed height. The amount of energy absorbed by the notched Charpy bar can be measured by the maximum height to which the pendulum rises after breaking the sample. A Charpy V notch (CVN) test is not normally used for a cast iron inspection due to the fact that the graphite flakes in the cast iron constitutes notches that already has the material, and for that the test shows small change in the absorbed energy during the impact of the hammer.

4.5.- ULTRASOUND TEST

Ultrasonic inspection is a nondestructive evaluation method in which a beam of high frequency acoustic energy are

introduced into the material under evaluation in order to detect surface and subsurface flaws and to measure the thickness of the material or the distance to a flaw. When a disc of piezoelectric material is contacted to a block of cast iron, either using cement or by a film of oil as a couplant, and a high-voltage electrical pulse is applied to the piezoelectric disc, a pulse of ultrasonic energy is generated in the disc and is propagated into the material. This pulse travels through the metal and will be reflected at any surface or internal discontinuity in the specimen.

Considering that sound is a phenomenon which does not cause any permanent changes into the material being tested although its transient presence is very noticeable, and sound with low energy is suitable for nondestructive testing, because it permits obtaining exact information of the condition of the specimen being tested without any change in the structural condition of the piece material.

The entire ultrasound test is based on how the sound waves are influenced when they propagate within the material being tested. In other words, one can interpret certain changes in the sonic signal as a change in the structure of the material.

4.4.1.- PULSE-ECHO METHOD

The most important of all methods of ultrasound testing is the pulse-echo method, which using the signal reflected from a discontinuity or surface in the material, not only the size of the reflection indication (echo amplitude) can be

evaluated, but also the echo transit time, giving the position of the discontinuity or thickness. If the position of the reflector is know (e.g. back wall), then by using the transit time, the structure of the material can be evaluated by determining the velocity of sound, and from that velocity the mechanical properties of the material can be estimated.

4.4.2.- ULTRASONIC PROBES

The ultrasonic testing of materials cannot be carried out without the probes, and instrument which generates and receives ultrasound waves. For the generation and reception of sound waves in the pulse echo method, piezoelectric plates are frequently used and are made from various ceramic materials such as barium titanate, lead-metaniobate,lead-zirconate,etc.[13] The piezoelectric material transform the electric pulse to mechanical vibration,and the opposite. A damping element on the back of the crystal (and also coupling the probe to the test specimen) dampens the oscillation of the piezoelectric plate producing the ultrasonic pulse. If the damping is weak the pulse is long and its frequency spectrum is narrow band. Heavy damping produces short broad band pulses which in turn offer a high resolution for normal applications.

Calibration blocks from two locations in each of the four castings (see sketch in Figure # 5) were cut and then machined using a vertical-spindle rotary-table surface grinder machine, with an extreme accuracy of size and parallelism to better than 0.0001 mm per mm (0.0001 in. per inch) and a surface

finish of 0.25 mm (10 micro-inch).[14]

Knowing the sample thickness, the sound velocity was determined for each sample. The instrument used was the Epoch 2002 digital ultrasonic flaw detector made by Panametrics, Inc. Different transducers were used with frequencies 0.5, 1.0, and 2.25 MHz.

4.6.- METALLOGRAPHY

The various forms in which graphite occurs in cast iron has been classified into seven basic types in the ASTM A-247 and shown in the Figure # 6.[12] The Type I graphite is the usual form that occurs in ductile iron although the presence of Type II forms has a little or no effect on the properties of ductile iron. The Type III graphite is the usual form most often seen in the malleable iron after the heat treatment. Type IV is the main type in compacted graphite iron. Types V and VI occurs in ductile iron when some incomplete inoculation treatment has been done. Type VII is the flake graphite form that occurs in gray iron.

The flake graphite form has been further classified in five different shapes, A through E, as in the Figure # 7. The A flake graphite has a uniform distribution and apparent random orientation. It is the commonly preferred type for mechanical applications. Graphite in rosette groupings is called the type B. This occurs in irons near the eutectic composition and the centers of the rosettes generally show fine graphite which is formed as result of some degree of

undercooling during solidification. When the temperature is raised because of the latent heat of solidification, the graphite grows in normal manner.

Type C flake graphite occurs in hypereutectic irons. This coarse graphite is desirable in applications involving heat transfer as in ingot molds. Type D occurs in metal that was rapidly cooled but with sufficient silicon to prevent the retention of iron carbide. The type E graphite occurs in low total carbon irons. The graphite is confined to the interstices between the austenite dendrites so the graphite is classified as interdendritic with a preferred orientation. In addition, the specification A-247 contains requirements for the size of the graphite in both the flakes and nodular form. A chart establishes sizes from one to eight for comparison with a sample of casting viewed at the microscope at 100x is given in the Figure # 8.

Samples for metallographic studies were prepared from the broken tensile bars, the Charpy bars, wall cross sections, and from the lift-lugs. The procedure followed was selected from the literature[3,4,15]. After a carefully study of the samples in the optical microscopy, and due to the size of the graphite flakes, some modifications were introduced and its main difference is to polish the samples in diamond abrasive paste of sizes of 6, 3 and 1 micron, without the rotation of the wheel, in a short-nap cloth.

4.7.- Eddy Current

Eddy current testing utilizes the observation of the interaction between the electromagnetic field and the metal to measure the combination of the inductance and electrical resistance of the iron.[13] The test results can be correlated with metallurgical variables in the specimen, and is particularly useful in indicating the amount of ferrite and pearlite in the matrix, and thus is an indication of the hardness.

The Eddy current test was done with the Nortec NDT-3 equipment using the 100 KHz probe, in the same coupons prepared for ultrasound test.

5.- RESULTS

5.1.- CHEMICAL COMPOSITION

The results of four different casting chemical composition are indicated in the Table # 1.

5.2.- HARDNESS

The Rokwell B Hardness (HRB) results from the tensile coupons are indicated in the Tables # 2a y 2b.

5.2.- TENSILE TEST

The results of the tensile test are indicated in the Table # 2a and 2b.

5.3.- IMPACT TEST

The results of the impact test are indicated in the Table # 3.

5.4.- ULTRASOUND TEST

The results of the sound velocity measured with the different transducers are indicated in the Table # 4. It is possible to notice that the change in sound velocity value is too small (less than 0.0005 in/micro sec) that the sound velocity could be considered constant for the different transducers frequency.

The change in sound velocity with the microstructure of the casting could be noticed in the different samples as appears in the Table # 7. It is important to notice that the sound velocity increase with the tensile strength of the

samples, as shown in the Figure # 4.

5.5.- METALLOGRAPHY

The results of the metallographic study are presented in the Figures # 9 to Figure # 24, and in Table # 5.

5.6.- Eddy Current

The results of the Eddy current testing appears in the Table # 6.

6.- DISCUSSION

6.1.- METALLOGRAPHY

The cross section metallography of the castings in the Figures # 21 to 24 show a chill zone at the external surface of the casting corresponding to a pearlite structure of 0.05 mm (0.002 inch) thick . Below this chill zone, the cast iron structure appears formed of small rosettes of carbon flakes of type B and size number 4 and 5, in a thickness of 2.5 mm (0.1 inch). This structure of rosettes could be formed by the undercooling produced and the rapid solidification rate obtained.

Finally, the central zone of the casting most of 37.5 mm (1.5 in) thickness, it has the basic structure of big carbon flakes of graphite of type A and size number 1 and 2. The matrix in the central zone of the cross section is formed by a mixture of pearlite-ferrite microstructure and the ratio in function of the chemical composition and cooling rate during the solidification of the casting.

The metallographic study show that the microstructure of the samples choose were of cast iron with the carbon free in form of graphite flakes basically of the type A and a size of the flakes number 1 or 2, corresponding to the biggest in the classification given by the standard ASTM A-247 (Figure # A25

of the Appendix 1). The matrix is composed of a mixture of ferrite and pearlite microstructure.

In addition to this phases present, it is possible to notice the presence of the Manganese Sulphide (MnS) entrapped in random position in the matrix as show in the Figure # 23. In the same way the microstructure show the presence of steadite, which is a hard eutectic constituent of γ Iron and Iron-Phosphide (Fe_3P) as show in the Figure # 10. The eutectic consists of 10.2 weight % P and 89.8 weight % Fe.[15] This eutectic clearly appears entrapped between the dendrites of austenite (transformed into pearlite) destroying the continuity of the matrix and making the casting more fragile than usual.

6.2.- CHEMICAL COMPOSITION

The chemical composition of the castings in comparison with the typical composition of gray iron given in the Metals Handbook[16] , Table # 7, with the same thickness, show some important differences. First the total carbon content of the samples is higher the range stated for the Class 20 heavy section 2.5 cm (1 in) thickness, with the exception of the casting B2, which is the only one that has the total carbon content within the given range. Second, it is clear that the higher total carbon of the casting results in lower tensile strength of the casting, and the same relationship holds with the carbon equivalent. The carbon equivalent concept is used

to evaluate the effect of the chemical elements added to the casting since these elements help in the formation of graphitic carbon and is given as:

$$C\ eq = C\ total + (Si + P)/3.$$ [17]

Again from the study of the values of carbon equivalent is clear that the casting B2 is the only one which has the value similar to those given in Table # 7.

From the observation of the combined carbon in the Table # 1, it is possible say that the combined carbon of castings A2 and B1 are approximately equal,(A2 and B1 have similar tensile strength) while the castings A3 and B2 are similar too. The carbon graphitic content is high for the castings with low tensile strength such as the castings A2 and B1.

In summary, it is clear that the chemical composition of the castings made at the early years of the 20th century differ greatly from castings made in the second half of the 20th century, with the old castings having low values of mechanical properties.

6.3.-TENSILE STRENGTH

The results of the tensile test, Table # 2, show clearly that the castings could be grouped in two different subgroups, the two with the low values of tensile strength corresponding to the castings A2 and B1, and the group of higher tensile strength corresponding to the castings A3 and B2, and inside of this subgroup the highest value corresponding with the casting B2.

The tensile strength of the walls of the casting are higher than the ribs of the castings, instead of the similar value of tensile strength which would be expected due to the similar thickness of the two parts. This difference occurs because of the solidification rate was different, and the solidification direction is different too. In the case of the ribs, the tensile coupons apparently were taken perpendicular to the direction of the dendritic growth. The tensile coupons from the walls had been machined parallel to the dendritic growth and this gave higher value of the tensile strength.

The fact that mechanical properties are strongly influenced by the size and morphology of graphite could be seen when you compare the samples A2 and B1 (Figure # 13 and Figure # 15 respectively) in which the matrix microstructure is almost the same, but the difference in the graphite flakes are bigger in the case of the casting B1 which results in lower tensile strength. The same occurs with the samples A3 and B2, which almost have the same amount of combined carbon in the microstructure, the high strength of the casting B2 is because of the smaller size and better distribution of the graphite compared with the casting A3.

CORRELATION

At this point is interesting make an initial correlation between the parameters studied. The chemical composition shown the combined carbon of the castings A2 and B1 to be a low value, and the same castings have a low values of tensile

strength. Looking the values for samples A3 and B2, the same relation is obtained, high combined carbon gives high tensile strength. Notice that the combined carbon is the measure of the amount of carbon present in the form of pearlite, and from that is possible to say that the higher the amount of pearlite the higher the tensile strength of the casting.

Not only the amount of combined carbon is important in this relationship, but also the amount of graphite. From the observation of the graphitic carbon in the Table # 1 of chemical composition and Table # 2 of tensile strength of the castings, it is possible to say that the lower the graphitic carbon the higher the tensile strength of the casting. In other words, given the same combined carbon and graphitic carbon in two different samples, the final tensile strength depends in the distribution,type and size of the graphite in the microstructure.

6.4.- ULTRASOUND

Due to the age of the tunnel, it is desire to evaluate the structural parts with the least destructive technique possible, and that is why the use of nondestructive evaluation (NDE) are of importance. From the broad spectrum of NDE techniques and because of many of the tunnel liner sections have access to only the inner surface, the ultrasound technique (UT) was chosen as good alternative with the principal objective of thickness measurement of the casting walls.

Using UT equipment normally designed for the thickness measurement in materials such as steel,aluminum,copper, etc, the results on cast iron were not good because these equipment use transducers of high frequency typically 2.25 to 5.0 MHz. At high ultrasonic frequencies, transducers produce ultrasound with very small wave lengths, these short wave lengths makes it difficult for the sound wave to pass through or around the graphite flakes of the cast iron and reach the transducer after reflection from the far wall, and this is why the back reflection of the signal from cast iron is almost impossible to distinguish from the background signal in the cathode ray tube (CRT) (e.g. no back wall reflection is found in cast iron).

From the knowledge of the microstructure of these cast iron castings which have very big graphite flakes, it was decided to use the ultrasound technique but with low frequency transducers which gives longer wave lengths. The longer wave length is able to pass through and around the graphite flakes and gives a good back reflection, making possible the determination of the casting wall thickness. Transducers of 0.5 and 1 MHz were selected as the more appropriate because of the high definition of the back reflection signal in the CRT. In addition the lower frequency of the transducer results in a reflected signal higher in amplitude showing less attenuation.

Analyzing the sound velocity data obtained from the

different samples, Table # 4, and making a correlation with the tensile strength data, Table # 2, it is clear that a general relationship between sound velocity and tensile strength and hardness, as show in Figures 26 y 27, is not simple for this material principally due to the effect of the graphite flakes and porosity on the movement of the ultrasound wave.

As is well known, in cast iron the chemical composition, solidification rate, and the process itself, are variables that affect the final microstructure of the piece such as the pearlite-ferrite ratio, size of the cell, and the size,shape and distribution of the graphite inside of the cell. Because of this characteristic of the cast iron, it was necessary to select from the whole casting one section which should have had similar solidification rates. The hook lifters (see Figure # 5) were chosen to provide a good data of the sound velocity of the different casting.

It is important to state that in gray iron castings the microstructure changes from one to other structure in a fraction of an inch, making it very difficult to obtain a unique microstructure representative of the whole. This microstructural variation is the reason why the sound velocity may be different from one point in a casting to the other. Complicating a little more this situation are the presence of the casting defects such as porosity and micro-shrinkage (air and vacuum have lower velocity of the sound) that

decrease the value of the sound velocity obtained.

Nevertheless, the decrease in the sound velocity, as shown in the Table # 4, with the increase of the porosity and micro-shrinkage of the casting could be used to distinguish a defective area from a sound area. In other words, the change in sound velocity due to defective areas could be used as quality control procedure. If the sound velocity is measured between two points in the casting, this value should be high when the casting is defect free, but the data should be lower in value when a defective area is present between the two points.

6.5.- The Impact Test

Charpy notched impact test was done for the different casting. The coupons were extracted from the same equivalent area and machined to standard dimensions in two different directions, one parallel to the direction of liquid metal flow into the casting, and one perpendicular to it. The test was done at room temperature (23°C). From the results of the Charpy notched impact tests, given in the Table # 3, it is possible observe that the impact energy absorbed by the material is very low around 1.63 joule (1.2 ft-pound), and all the samples show almost the same value of impact energy. The results do not show any difference between longitudinal and transversal directions.

The reason for the low value of impact energy could be done to the fact that the graphite flake structure allows

fracture to occurs with very little plastic deformation. Therefore, the principal energy absorbed in the fracture is the elastic energy as the specimen is stressed to a level where fracture occurs. Also the presence of the external machined notch in the test piece, does not change the nature of the gray iron fracture but simply reduces the amount of deflection of the test piece.[1] In other words, the cast iron material has hundreds of sharp notches inside of the material one of which easily could produce the crack initiation therefore, the external machined notch does not affect in the fracture mechanism.

6.6.- FRACTURE

The fracture analysis were done in the Charpy notch impact bars of the different castings and look for the pattern of the fracture mode . As is shown in the Figures #28 and 29, the fracture of this kind of material (as expected) should be classified as a brittle fracture. The fracture mode in the matrix correspond to the cleavage mode as illustrated in the Figure # 29, were it is possible observe the cleavage planes. The initiation of the fracture appears to be the graphite flakes and then moves to the matrix of the material, initially by cleavage mode and finally using the quasi-cleavage mode (transition mode). In addition it is possible to observe in the Figure # 28 the presence of small areas of a eutectic structure corresponding to the fracture of the steadite, the

eutectic of iron-iron phosphide. Also the presence of small particles corresponding to the manganese sulphide were noticed.

In the Figures # 30 and 31, the fractographs shows the micro-shrinkage region of the casting, where it is possible observe the holes produced by the contraction of the liquid-solid transformation. A magnification of the broken dendrites show a fracture initiation in the flakes of graphite and then the growing fracture by cleavage into the matrix of the casting.

The Electron-microscopy study shows that the fracture surface corresponds to a brittle fracture in the cleavage mode, and that due to the morphology of the graphite flakes, it constitutes a big discontinuity in the matrix of the metallic material.

7.- CONCLUSIONS

7.1.- Old gray iron castings have chemical composition which are similar to the range of typical compositions. Nevertheless, old gray cast iron casting have tensile strength which are lower than the typical values for recently produced gray cast iron castings. The lower strength appears to be related to the large graphite flake size.

7.2.- The use of low frequency transducers improves the signal in the CRT of the ultrasound equipment in the cast iron evaluation, so that ultrasound testing is a suitable technique for a cast iron evaluation.

7.3.- A high ultrasound velocity for the iron casting testing, is directly related with the high tensile strength. At high ultrasound velocity corresponds a high tensile strength, and at low ultrasound velocity corresponds a low tensile strength.

7.4.- The ultrasound technique appears to be useable technique for the evaluation of actual conditions of the cast iron material used in old civil engineering structures.

TABLE # 1

CHEMICAL COMPOSITION OF CASTINGS

(Weight %)

Element	Casting A2	Casting A3	Casting B1	Casting B2
C (total)	3.66	3.52	3.49	3.24
Mn	0.47	0.65	0.56	0.54
P	0.324	0.414	0.248	0.287
S	0.044	0.031	0.069	0.046
Si	1.29	1.55	1.36	1.08
Mo	0.03	0.04	0.03	0.04
Cu	0.02	0.03	0.03	0.03
N	0.023	0.040	0.028	0.025
C eq	4.2	4.17	4.026	3.69
C combined	0.28	0.58	0.29	0.55
C graphite	3.35	3.00	3.41	3.22

* C eq = Carbon equivalent

TABLE # 2a

TENSION AND HARDNESS RESULTS FROM WALLS OF CASTINGS

CASTING	YIELD STRENGTH psi	(MPa)	TENSILE STRENG. psi	(MPa)	ELONG % 2"	HARDNESS HRB
A2-1W	11 429	78.80	12 236	84.37	1.9	40
A2-5W	12 992	89.58	14 456	99.67	1.4	45
Avg	**12 210**	84.19	**13 346**	92.02	1.6	43
A3-3W	15 936	109.88	17 678	121.89	0.9	71
A3-4W	16 565	114.21	19 541	134.73	2.2	70
A3-9W	15 910	109.70	18 506	127.60	0.8	69
A3-10W	16 064	110.76	18 369	126.65	1.3	68
Avg	**16 118**	111.13	**18 532**	127.77	1.3	69
B1-1W	12 030	82.94	13 414	92.45	0.9	40
B1-6W	10 904	75.18	12 322	84.96	1.3	44
Avg	**11 467**	79.06	**12 868**	88.72	1.1	42
B2-1W	17 744	122.34	19 263	132.82	1.6	68
B2-3W	16 895	116.49	18 917	130.43	1.6	70
B2 7W	16 775	115.66	18 832	129.85	1.3	66
B2-10W	16 301	112.39	19 063	131.44	1.6	70
B2-11W	17 014	117.31	19 001	131.0	1.4	72
Avg	**16 945**	116.83	**19 015**	131.11	1.5	70

TABLE # 2 b

TENSION AND HARDNESS RESULTS FROM RIBS OF CASTINGS

CASTING	YIELD STRENGTH psi	(MPa)	TENSILE STRENG. psi	(MPa)	ELONG % 2"	HARDNESS HRB
A2-1R	12 079	83.28	13 488	93.0	1.5	
A2-5R	12 481	86.06	13 452	92.75	1.8	
A2-6R	13 085	90.22	14 293	98.55	2.9	
A2-9R	12 531	86.40	13 584	93.66	2.0	
A2-10R	12 331	85.02	13 759	94.87	2.1	
A2-1-2R	13 433	92.62	14 130	97.43	1.3	
Avg	**12 657**	87.27	**13 784**	95.04	1.9	
A3-2R	14 229	98.11	17 823	122.89	1.1	68
A3-3R	13 504	93.11	15 358	105.89	1.2	68
A3-9R	12 881	88.81	14 863	102.48	1.6	64
A3-10R	14 678	101.20	16 870	116.32	1.4	67
Avg	**13 823**	95.30	**16 228**	111.89	1.3	67
B1-1R	9 524	65.66	11 830	81.57	2.0	
B1-5R	9 812	67.65	10 937	75.41	3.5	
B1-6R	9 990	68.88	11 713	80.76	1.5	
B1-9R	10 569	72.87	11 475	79.12	1.4	
B1-10R	10 025	69.12	11 328	78.11	1.9	
B1-1-2R	9 851	67.92	11 368	78.38	2.5	
Avg	**9 962**	68.69	**11 441**	78.88	2.1	
B2-5R	13 630	93.98	16 176	111.53	1.7	68
B2-6R	16 782	115.71	19 464	134.2	1.8	70
B2-10R	13 779	95.0	15 856	109.33	1.9	66
Avg	**14 730**	101.56	**17 163**	118.34	1.8	68

TABLE # 3

RESULTS FROM NOTCHED BAR IMPACT TEST
(ASTM E-23)

CASTING	ENERGY Ft-Lb (joule)		CASTING	ENERGY Ft-Lb (joule)	
A2-L1	1.2	1.672	B1-L1	1.12	1.518
A2-L2	1.16	1.573	B1-L2	1.36	1.844
A2-L3	1.28	1.735	B1-L3	1.36	1.844
A2-L4	1.12	1.518	B1-L4	1.2	1.672
A2-T1	1.04	1.41	B1-T1	1.20	1.672
A2-T2	1.53	2.075	B1-T2	1.12	1.518
A2-T3	1.2	1.672	B1-T3	1.28	1.736
A2-T4	1.15	1.56	B1-T4	1.29	1.75
A3-L1	0.96	1.30	B2-L1	1.44	1.953
A3-L2	1.20	1.672	B2-L2	1.60	2.17
A3-L3	1.28	1.736	B2-L3	1.20	1.672
A3-L4	1.20	1.672	B2-L4	1.28	1.736
A3-T1	1.20	1.672	B2-T1	1.44	1.953
A3-T2	1.15	1.56	B2-T2	1.44	1.953
A3-T3	1.20	1.672	B2-T3	1.20	1.672
A3-T4	1.16	1.573	B2-T4	1.26	1.71

TABLE # 4

ULTRASOUND VELOCITY OF CASTINGS

TRANS / CAST	0.5 MHz * in/microsec (Km/sec)	1.0 MHz * in/microsec (Km/sec)	2.25 MHz * in/microsec (km/sec)	1.0 MHz @ in/microsec (km/sec)
A2	0.1688 (4.287)	0.1690 (4.292)	0.1691 (4.295)	0.1547 (3.929)
A3	0.1734 (4.404)	0.1735 (4.407)	0.1733 (4.400)	0.1454 (3.693)
B1	0.1617 (4.107)	0.1619 (4.112)	0.1623 (4.122)	0.1462 (3.713)
B2	0.1774 (4.506)	0.1775 (4.508)	0.1780 (4.520)	0.1537 (3.904)

* Sound velocity in dense area
@ Sound velocity in porous area

TABLE # 5a

GRAPHITE DETERMINATION FROM TENSILE BARS MID-THICKNESS
(ASTM A-247)

CASTING	FORM	TYPE	SIZE
A2-1W	VII	C	1
A2-5W	VII	C	2
A3-3W	VII	A	3
A3-4W	VII	A	3
A3-9W	VII	A	2
A3-10W	VII	A	3
B1-1W	VII	B	1
B1-6W	VII	B	1
B2-3W	VII	B	3
B2-7W	VII	B	4
B2-10W	VII	B	3
A3-2R	VII	A	3
A3-3R	VII	A	2
A3-9R	VII	A	2
A3-10R	VII	A	2
B2-5R	VII	A	3
B2-6R	VII	B	3
B2-10R	VII	A	2

TABLE # 5b

GRAPHITE DETERMINATION FROM THROUGH-WALL THICKNESS
(ASTM A-248)

CASTING	FORM	TYPE	SIZE	POSITION *
A2	VII	A	3	Inside
A2	VII	A-C	2	Middle
A2	VII	B	5	Outside
A3	VII	B	5	Inside
A3	VII	A	2	Middle
A3	VII	B	4	Outside
B1	VII	A	3	Inside
B1	VII	B	1	Middle
B1	VII	B	4	Outside
B2	VII	B	6	Inside
B2	VII	B	3	Middle
B2	VII	B	4	Outside

* INSIDE = Concave surface
Middle = Center of cross section
Outside = Convex surface

TABLE # 6

EDDY CURRENT RESULTS

(ohms)

	A2	A3	B1	B2
Reactance (X)	7.06	6.97	7.05	6.93
Resistance (R)	5.79	5.84	5.74	5.88

TABLE # 7

COMPOSITION OF GRAY IRON BASED ON STRENGTH

Type	Composition, % TC	Si	P	S	Mn	Average carbon equivalent(a)	Metal section range, in.	Brinell hardness number	Transverse load, lb	Transverse deflection, in.	Tensile strength, psi
Class 20, light section, 0.875-in. test bar	3.50 to 3.80	2.40 to 2.60	0.20 to 0.80	0.08 to 0.13	0.50 to 0.70	4.56 to ...	Up to 0.50	160 to 200	900 to 1200	0.10 to 0.15	22,000 to 26,000
Class 20, medium section, 1.2-in. test bar	3.40 to 3.60	2.30 to 2.50	0.20 to 0.60	0.08 to 0.80	... to ...	4.34 to ...	½ to 1	160 to 180	1600 to 2200	0.20 to 0.27	18,000 to 24,000
Class 20, heavy section, 2.0-in. test bar	3.10 to 3.30	2.20 to 2.40	0.20 to 0.40	0.08 to 0.13	0.50 to 0.80	3.98 to ...	1 and up	130 to 180	4500 to 6500	... to ...	18,000 to 22,000
Class 25, light section, 0.875-in. test bar	3.30 to 3.50	2.20 to 2.40	0.20 to 0.50	0.08 to 0.13	0.50 to 0.80	4.20 to ...	Up to ½	160 to 180	950 to 1300	0.11 to 0.16	25,000 to 29,000
Class 25, medium section, 1.2-in. test bar	3.20 to 3.40	2.20 to 2.40	0.15 to 0.40	0.08 to 0.12	0.50 to 0.80	4.08 to ...	½ to 1	172 to 207	1800 to 2400	0.22 to 0.28	26,000 to 29,000
Class 25, heavy section, 2.0-in. test bar	3.00 to 3.30	1.90 to 2.20	0.15 to 0.25	0.08 to 0.12	0.50 to 0.80	3.82 to ...	1 and up	179 to 217	6000 to 7800	... to ...	26,000 to 30,000
Class 30, light section, 0.875-in. test bar	3.20 to 3.40	2.10 to 2.30	0.15 to 0.30	0.08 to 0.12	0.50 to 0.80	4.03 to ...	½ to 1	179 to 228	1250 to 1500	... to ...	30,000 to 34,500
Class 30, medium section, 1.2-in. test bar	3.10 to 3.30	2.10 to 2.30	0.15 to 0.25	... to ...	... to ...	3.92 to ...	... to ...	... to ...	... to ...	... to ...	..... to .....
Class 30, heavy section, 2.0-in. test bar	2.90 to 3.20	1.70 to 2.10	0.15 to 0.25	0.08 to 0.12	0.45 to 0.70	3.68 to ...	1 and up	207 to 228	6500 to 8200	... to ...	30,000 to 34,500
Class 35, light section, 0.875-in. test bar	3.10 to 3.30	2.00 to 2.20	0.15 to 0.30	0.08 to 0.12	0.45 to 0.70	3.90 to ...	... to ½	179 to 228	1150 to 1450	... to ...	36,000 to 40,000
Class 35, medium section, 1.2-in. test bar	3.00 to 3.25	1.80 to 2.10	0.15 to 0.25	0.07 to 0.12	0.46 to 0.70	3.77 to ...	½ to 1	207 to 228	2300 to 3000	0.25 to 0.35	35,000 to 39,000
Class 35, heavy section, 2.0-in. test bar	2.80 to 3.10	1.60 to 2.00	0.10 to 0.20	0.06 to 0.12	0.45 to 0.70	3.54 to ...	1 and up	183 to 217	7500 to 9000	0.32 to 0.38	35,000 to 38,000

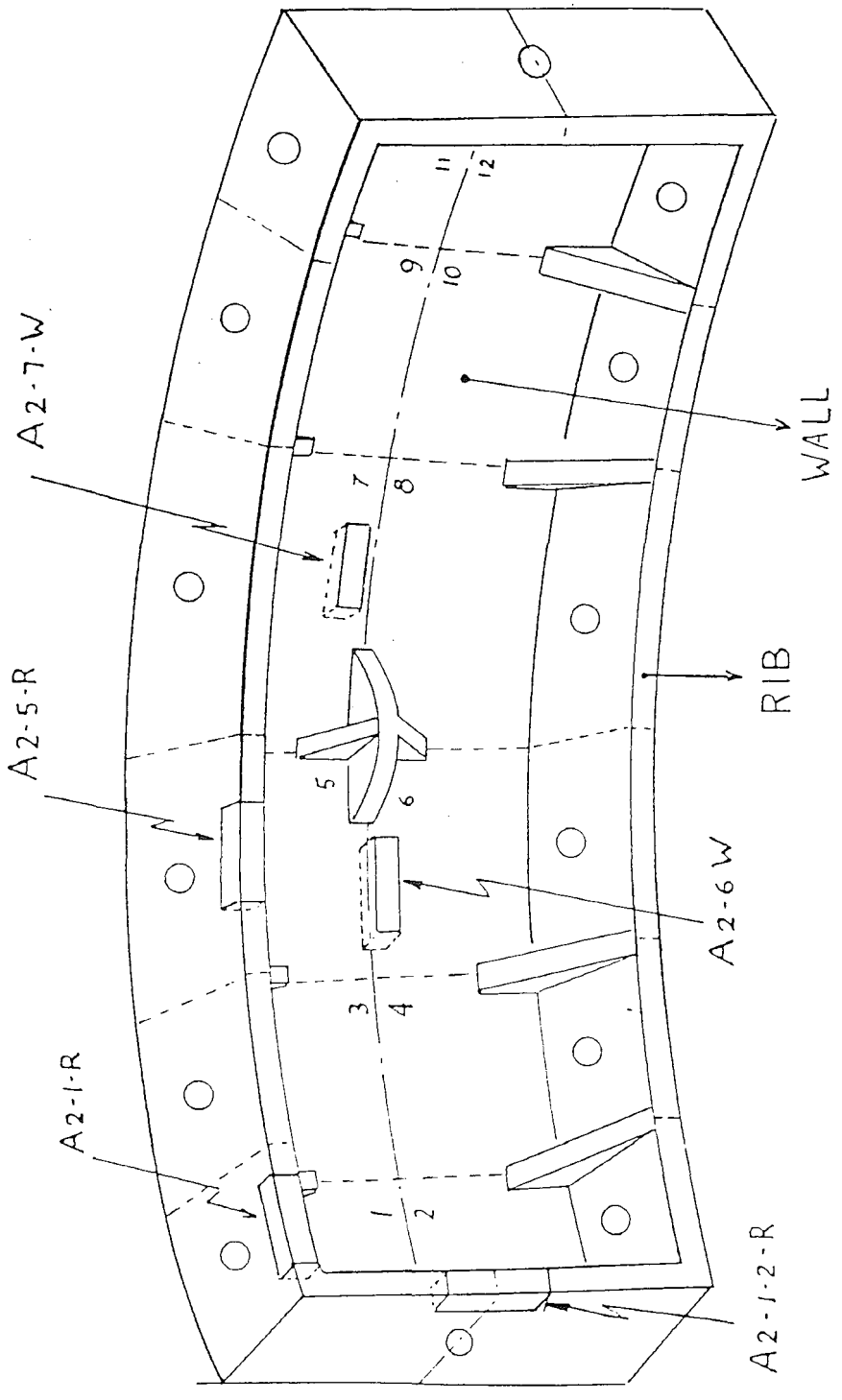

Figure # 1. Sketch of the casting showing the position of tensile coupons

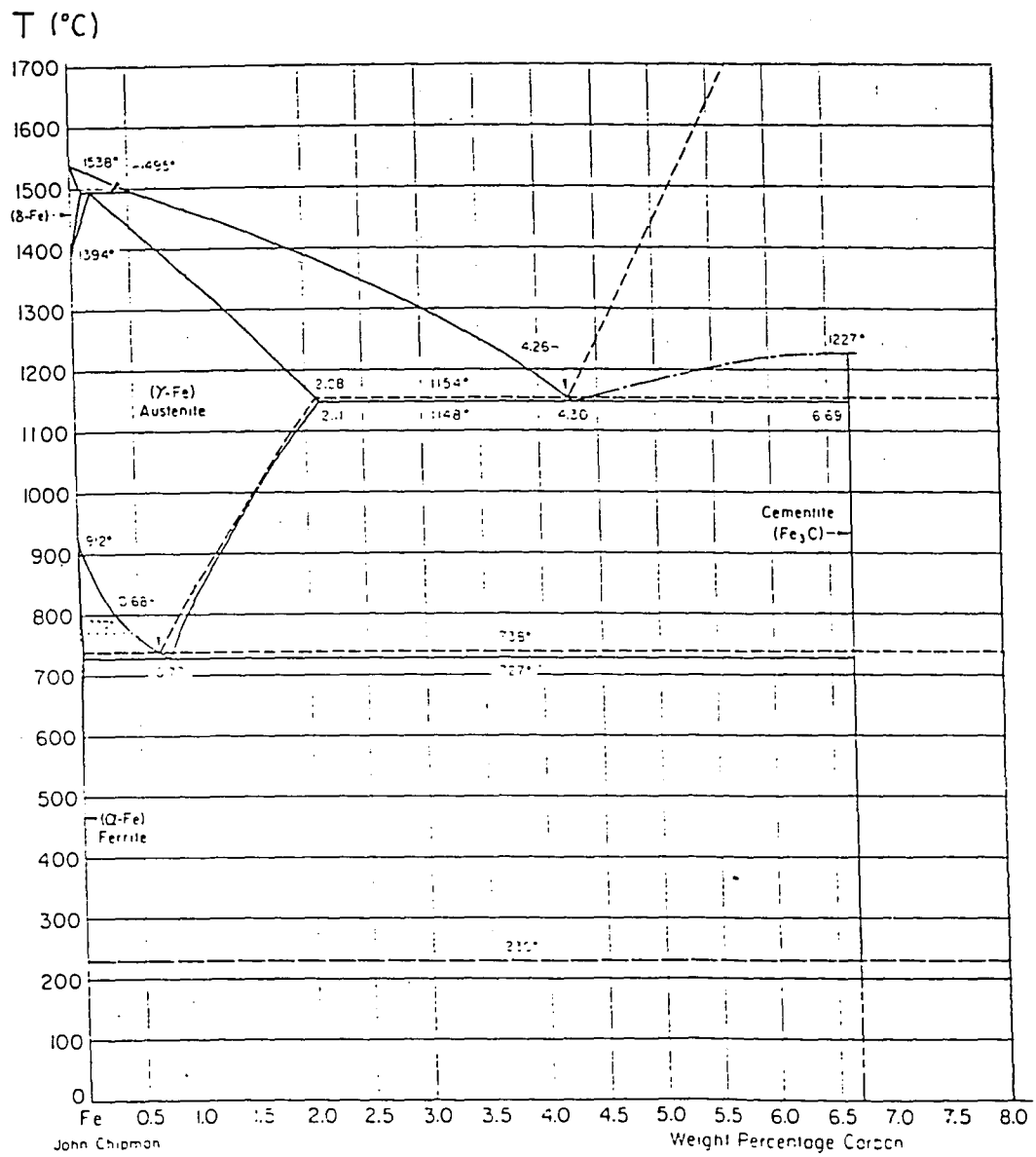

Figure # 2. Iron-Carbon Phase diagram[16]. The solid lines correspond the metastable Iron-Cementite system. The dashed lines, the stable Iron-Graphite system.

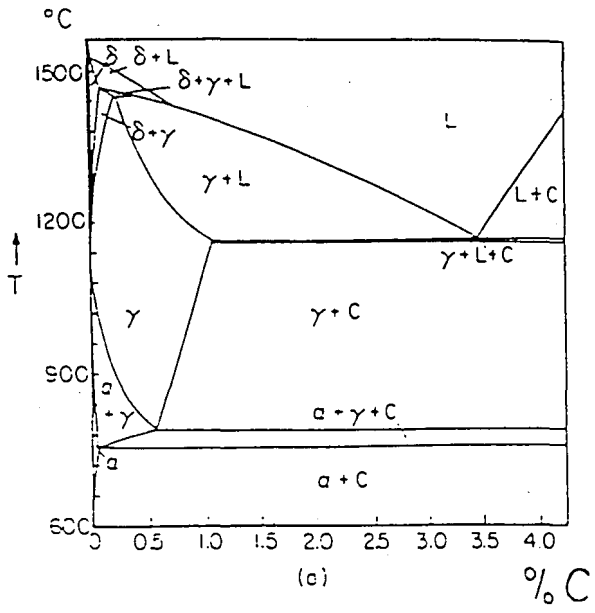

Figure # 3a. Vertical section of the Fe-C-Si diagram.[8]
(a) 2.4 % Si.

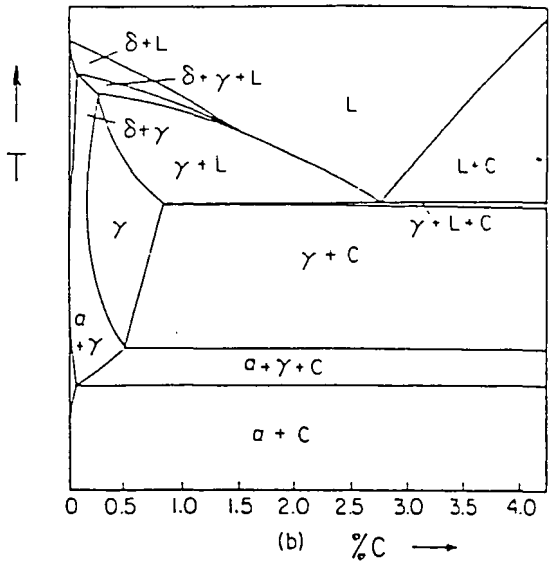

Figure # 3b. Vertical section of the Fe-C-Si diagram.[8]
(c) 4.8 % Si.

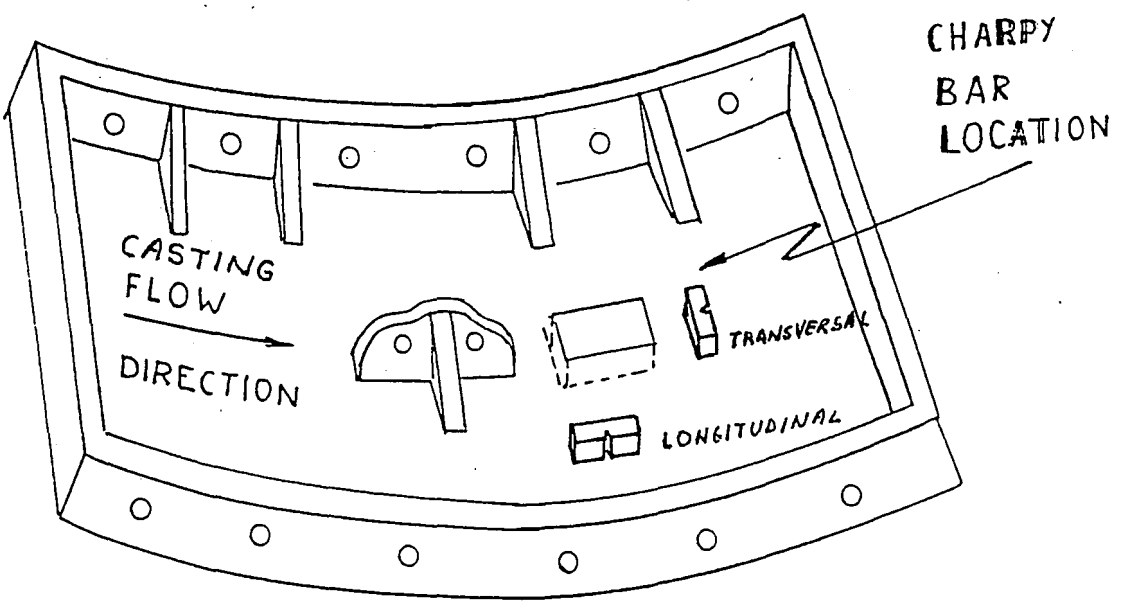

Figure # 4. Sketch of the location of Charpy coupons.

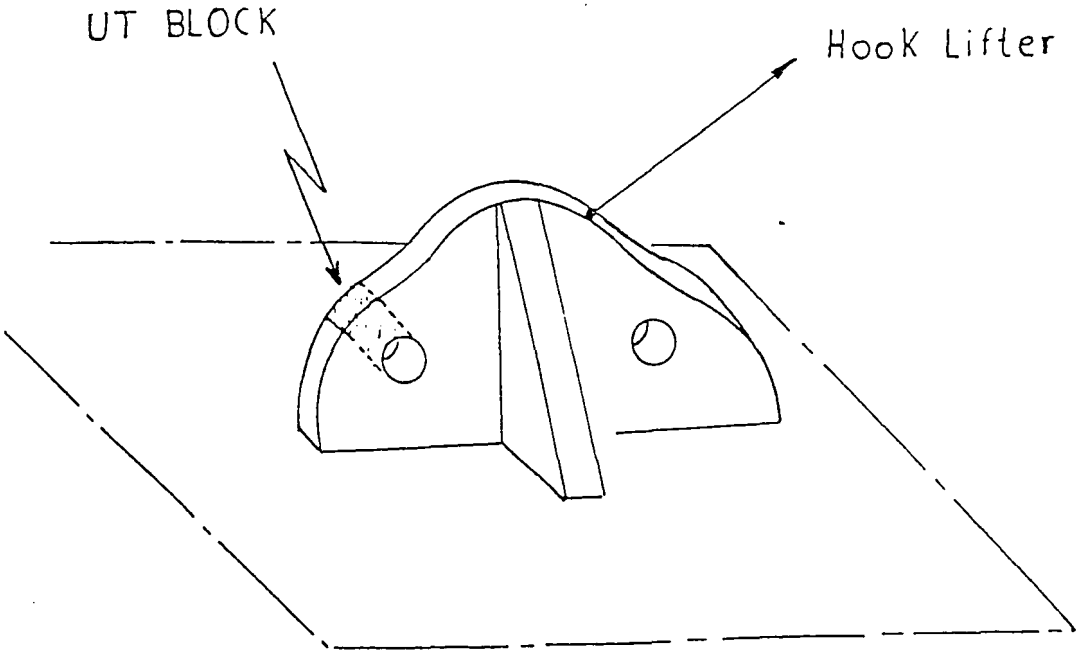

Figure # 5. Sketch of the position of ultrasound calibration blocks.

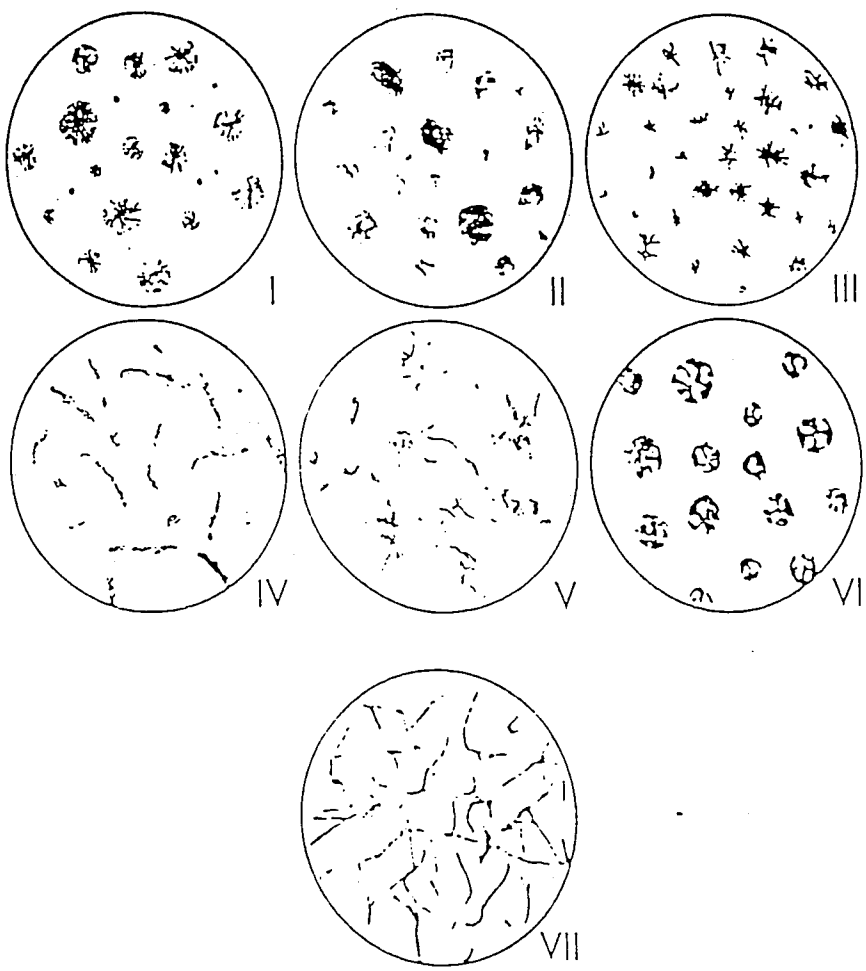

Figure # 6. Graphite type as established by ASTM A-247.[11]

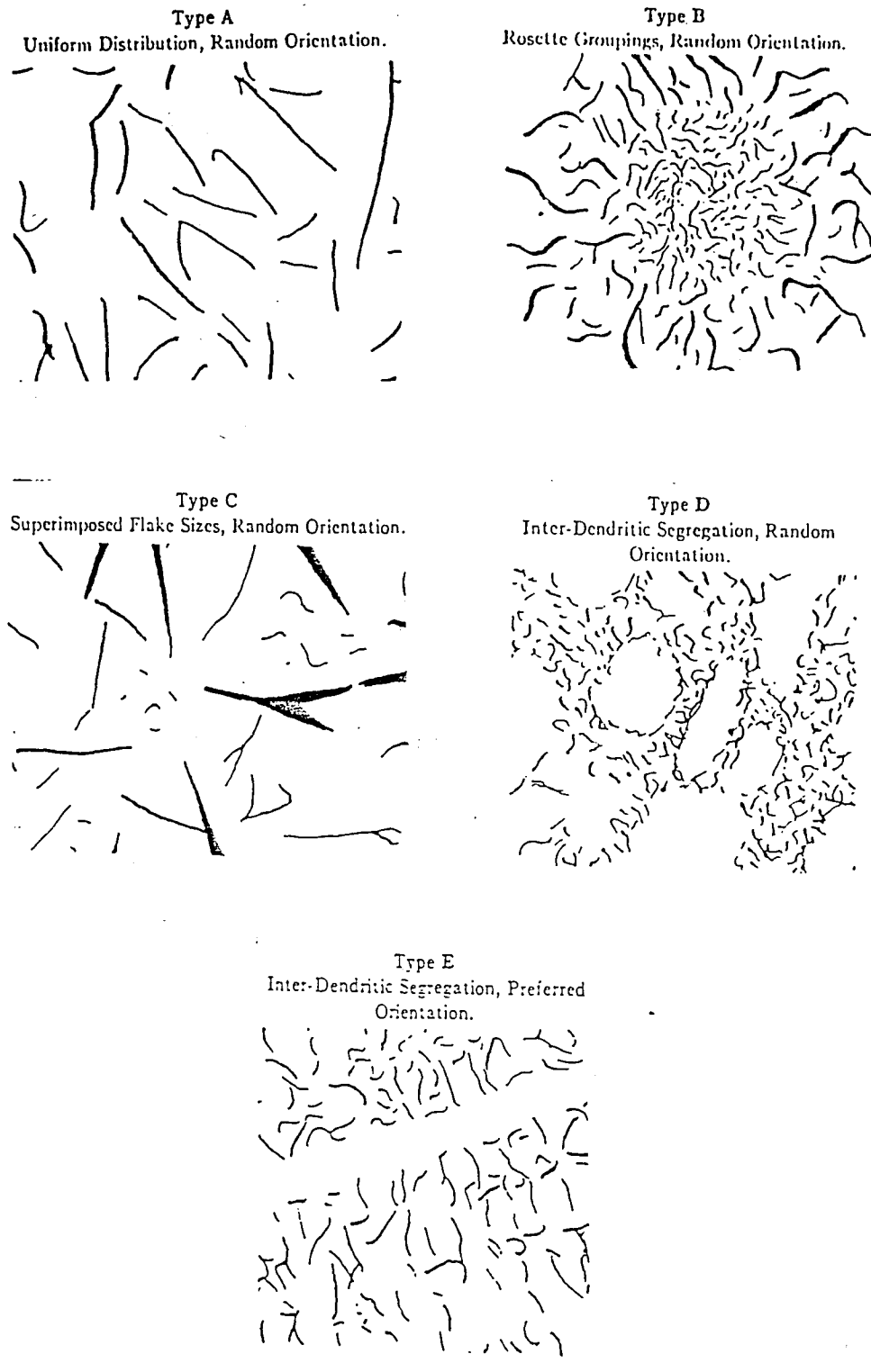

Figure # 7. The five types of flakes of graphite. ASTM A-247.[11]

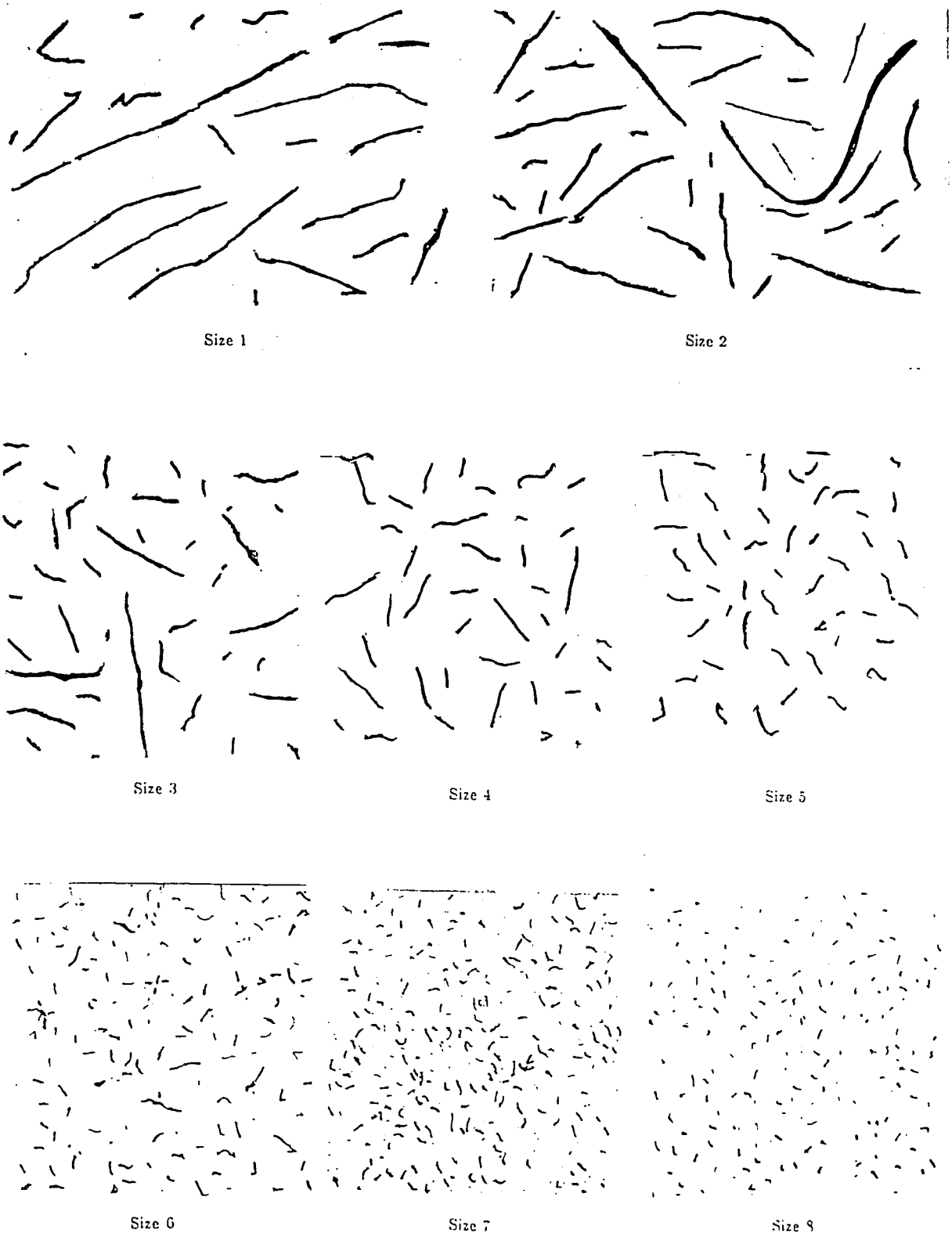

Figure # 8. Flake size chart for ASTM A-247.[11]

Figure 9 Microstructure of sample A2-Magnification:50X Etchant: Nital 2

Figure 10 Microstructure of sample A3-Magnification:50X Etchant: Nital 2

Figure 11 Microstructure of sample B1-Magnification:50X Etchant:Nital 2

Figure 12 Microstructure of sample B2-Magnification:50X Etchant: Nital 2

Figure 13 Microstructure of sample A2-Magnification:100X Etchant:Nital 2

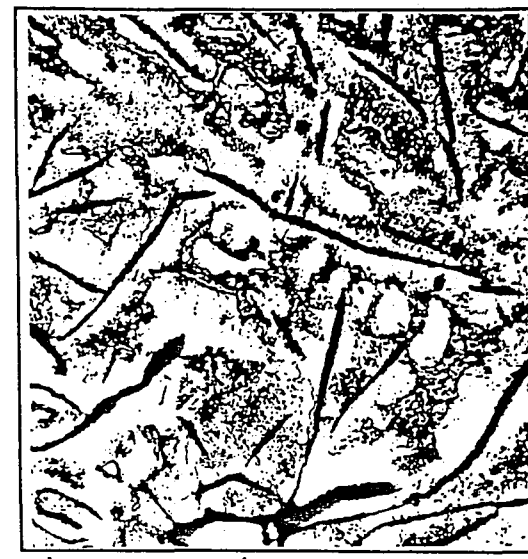

Figure 14 Microstructure of sample A3 - Magnification:100X Etchant: Nital 2

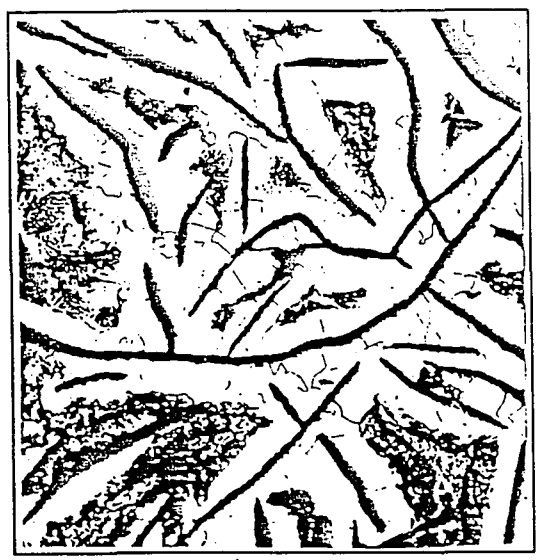

Figure 15 Microstructure of sample B1 - Magnification:100X Etchant:Nital 2

Figure 16 Microstructure of sample B2 - Magnification:100X Etchant: Nital 2

Figure 17 Microstructure of sample A 2 - Magnification:250X Etchant:Nital 2

Figure 18 Microstructure of sample A 3 - Magnification:250X Etchant: Nital 2

Figure 19 Microstructure of sample B 1 - Magnification:250X Etchant:Nital 2

Figure 20 Microstructure of sample B 2 - Magnification:250X Etchant: Nital 2

Figure 21 Cross section of wall of casting A2.
Concave surface.
Magnification: 100X
Etchant:Nital 2

Figure 22 Cross section of wall of casting A2.
Convex surface.
Magnification: 100X
Etchant: Nital 2

Figure 23 Cross section of wall of casting B2.
Concave surface.
Magnification: 100X
Etchant:Nital 2

Figure 24 Cross section of wall of casting B2.
Convex surface.
Magnification: 100X
Etchant: Nital 2

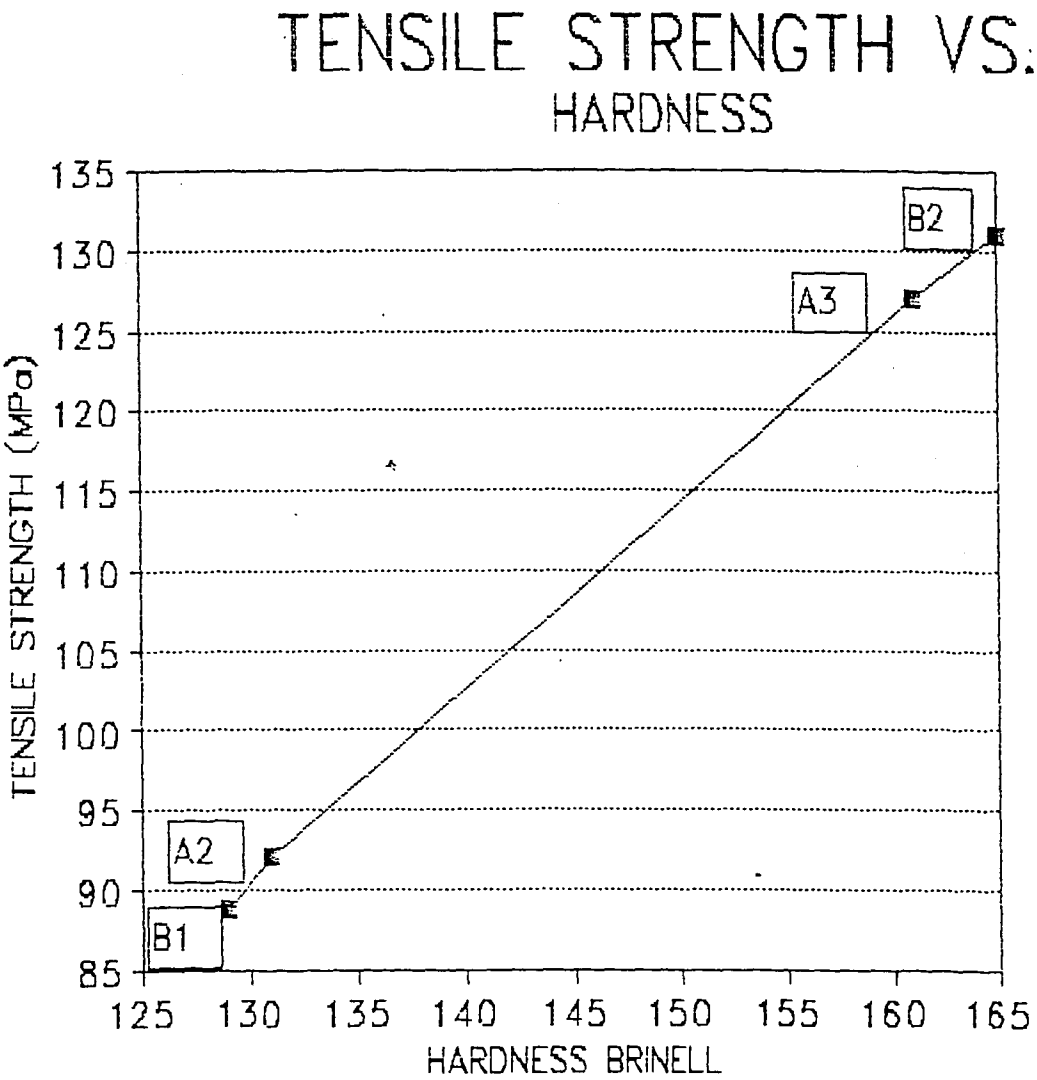

Figure # 25. Relation between hardness at the hook lifters and tensile strength of the different castings.

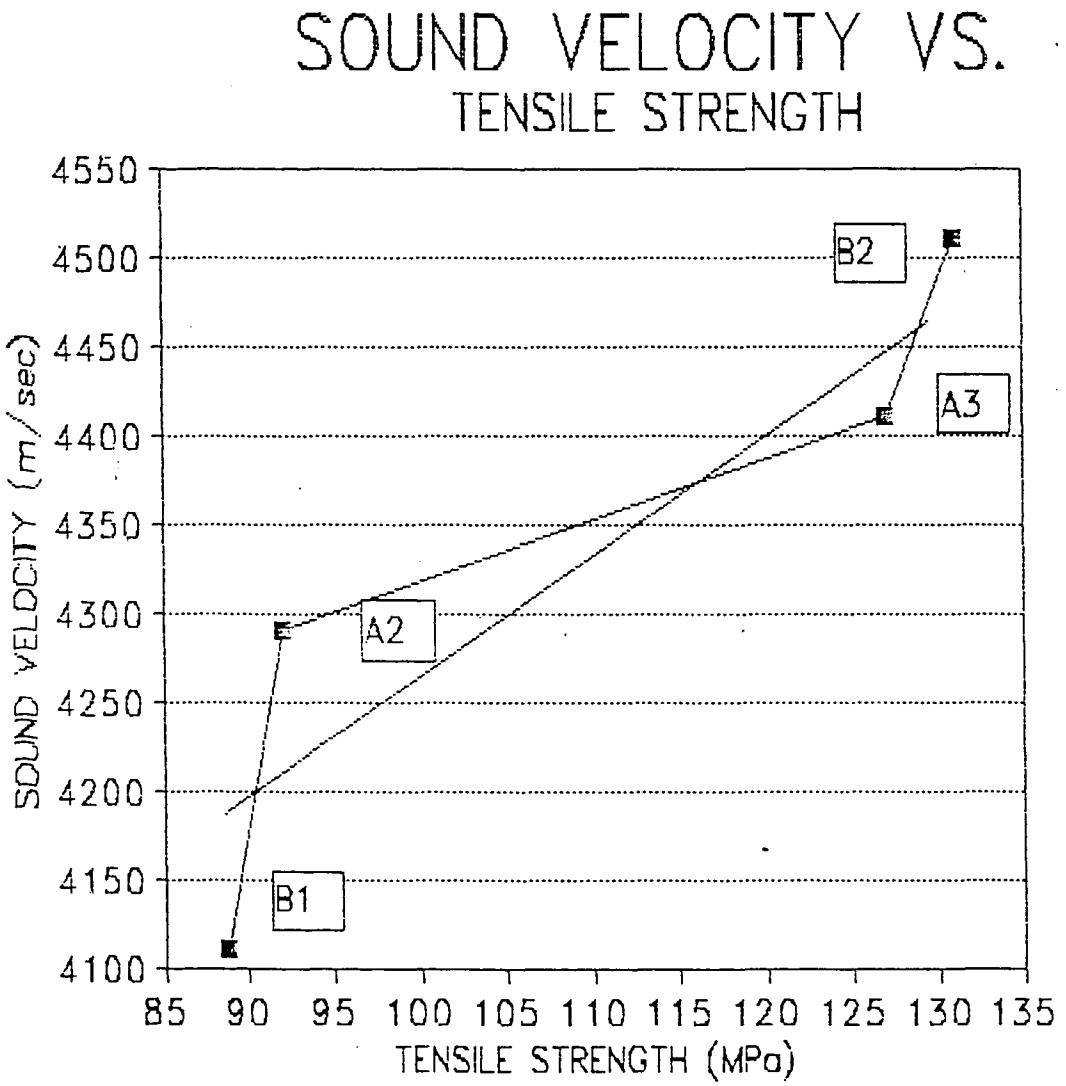

Figure # 26. Relation between sound velocity at the hook lifters and tensile strength of the different castings. The sound velocity increases as tensile strength increases.

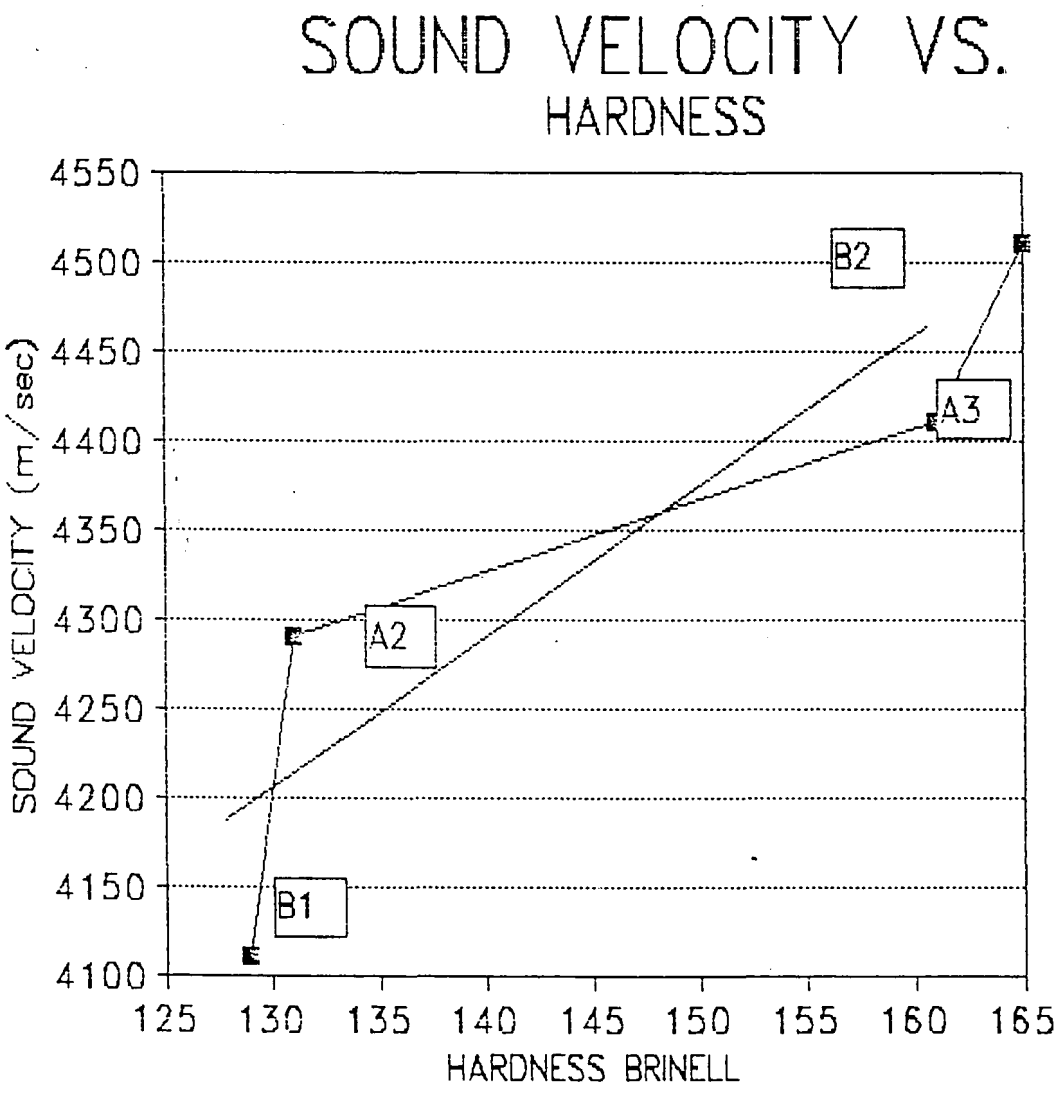

Figure # 27. Relation between sound velocity at the hook lifters and hardness of the different castings. The sound velocity increases as the hardness increases.

Figure 28. Fracture surface S.E.M. Sample B1. Magnification:60X

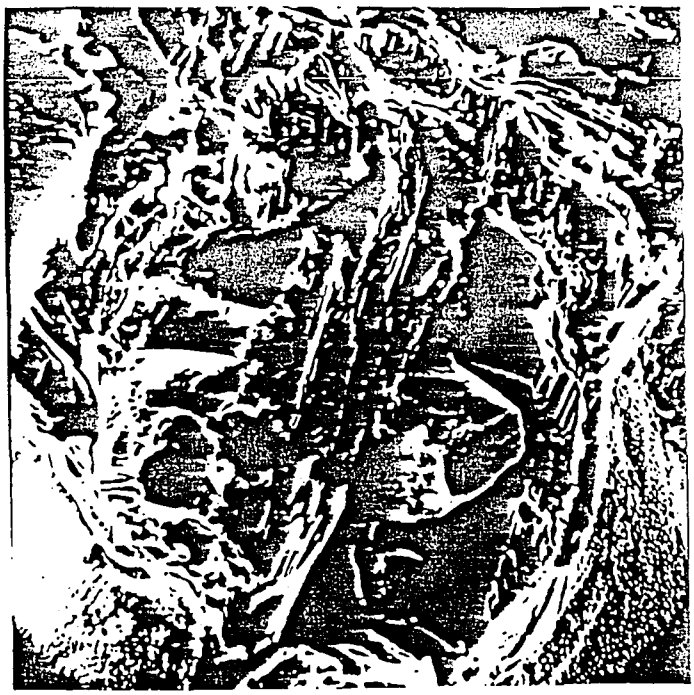

Figure 29. S.E.M. Fractograph surface same area as Figure # 28. Graphite flake, cleavage mode and quasi-cleavage. 900X

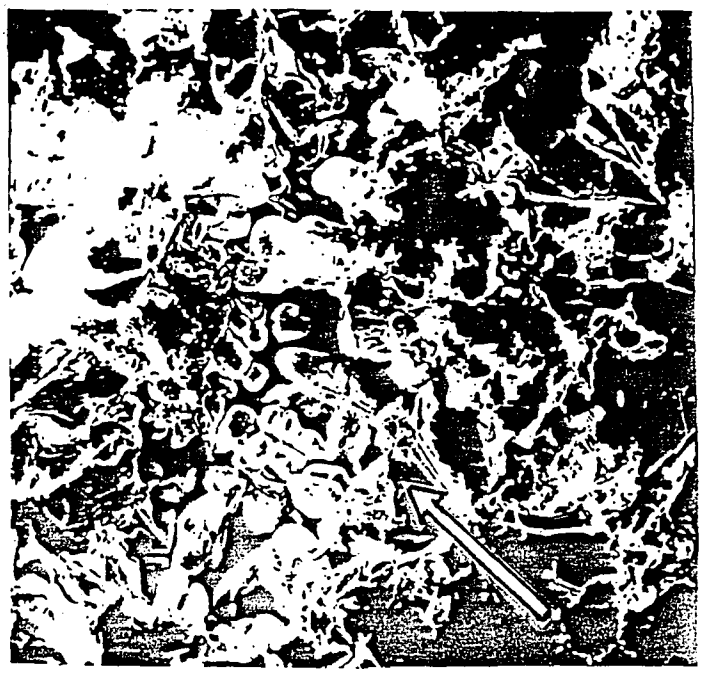

Figure 30. S.E.M. Fracture surface of casting A2. Micro-shrinkage area. Magnification: 40X

Figure 31. S.E.M. Same area as in Figure 25. Magnification: 300X

REFERENCES:

1.- Walton,C. Opar,T.; Iron Casting Handbook; Iron and Casting Society, Inc.; Chicago,1981.

2.- Brick,R.M.;Pense,A. and Gordon,R.B.;Structure and Properties of Engineering Materials; Mc Graw Hill,New York,1977.

3.- Saveur,A.; The Metallography and Heat Treatment of Iron and Steel; Mc Graw Hill, New York,1935.

4.- Hanemann,Heinrich; Atlas Melallographicus,; N.A. Pub. Berlin,1936.

5.- Minkoff,I.; The Physical Metallurgy of Cast Iron; John Wiley, New York, 1983.

6.- Hillert,M.;Suba Rao; The Solidification of Metals; The Iron and Steel Institute-110, London,1968.

7.- Hillert, M,; Recent Research on Cast Iron; E. Merchant; New York,1968.

8.- Sinha,A.K.; Ferrous Physical Metallurgy, Butherworths, Stone Ham,Mass.,1989.

9.- Neswagg,H. and Zuthoff,A.; The effect of S,P,Si and Al. on the Morphology and Graphite Structure of Directionally Solidified Cast Iron; Metallurgy of Cast Iron, Georgy Pub. Comp., Switzerland,1975.

10.- Standard ASTM A-48;American Society for Testing and Materials; Philadelphia, 1990.

11.- Standard ASTM E-8; American Society for Testing and

Materials; Philadelphia,1990.

12.- Standard ASTM A-247;American Society for Testing and Materials; Philadelphia,Pa, 1990.

13.- Halmshaw,R.; Non-Destructive Testing; E.Arnold Publisher; London, 1987.

14.- Metals Handbook, Vol 3,Machining, 8th Ed.; A.S.M.; Metals Park,Ohio, 1967.

15.- Metals Handbook, Vol.9,Metallography and Microstructures,9th ed.; A.S.M.; Metals Park, Ohio, 1985.

16.- Metals Handbook, Vol.8,Metallography, Structures and Phase Diagrams, 8th Ed.; A.S.M.;Metals Park, Ohio,1973.

17.- Handbook of Cupola Operation, American Foundrymen's Society; Mc Graw Hill, 1964.

18.- Porter,D.;Eastreling,K.; Phase Transformations In Metals and Alloys; Van Nostrand, New York,1981.

19.- Lundback,E.; Svensson,I.L.;Thorbrimssom,J.T.; Sodification Processing; The Institute of Metals,1987.

20.- Srinivasan,N. and Kondic,N.; The Metallurgy of Cast Iron; Georgy Pub. Co.;Switzerland,1975.

21.- Metals Handbook, Desk Edition, ASM; Metals Park, Ohio, 1985.

APPENDIX 1

THE PHYSICAL METALLURGY OF CAST IRON

1.- INTRODUCTION

Molten cast iron is very fluid, less reactive with air and molding materials, lower melting temperatures,and low cost than steels. The formation of lower density graphite during solidification causes the reduced volume change of the metal from the liquid to the solid. This permits the formation of complex castings such as one-piece water-jacketed internal combustion engine blocks without any shrinkage voids in the metal.

2.- Iron Carbon Phase Diagrams

For the study of cast iron, it is necessary to consider the two diagrams: the equilibrium phase diagram of iron-graphite or called the stable diagram, and the iron-iron carbide diagram that is not a true equilibrium diagram but is a metastable equilibrium diagram because the iron carbide or cementite is metastable phase (see Figure A1). Given a very long period of time, cementite will decompose into the equilibrium phases of graphite and iron by the reaction $Fe_3C = 3\ Fe + C$, were Fe_3C correspond to cementite, Fe is the ferrite and C the graphite. However for practical purposes, cementite must be treated as an equilibrium phase.

In the iron-carbon diagram[1] shown in the Figure # A1, the austenite phase (γ) is a solid solution of carbon in face centered cubic iron, with a maximum solubility of 2.11 weight % C . The carbon-iron (Fe-C) alloys with a carbon content up to 2.11 weight % are arbitrarily classed as steels and those beyond this amount are called as cast irons. Nevertheless, for practical purposes actually steels contain up to 1.1 weight % C. Inside of this range steels are divided in hypoeutectoid and hypereutectoid depending on whether the composition lies below or above the eutectoid composition of 0.77 %C. In the same way, the cast iron range may be subdivided into hypoeutectic or hypereutectic if the carbon content is below or above the eutectic composition of 4.3 weight %C, respectively. Usually the carbon content of cast iron vary from 2.3 to 4.3 weight percent.

The eutectic reaction shown in the Figure # A2, gives in full lines the graphite liquidus, while the dashed lines gives the cementite equilibria.[2] It is important to notice that the difference in temperatures of the two eutectics is of 6° C , the temperature range in which the graphite alone can nucleate, below 1148° C both eutectics, austenite -cementite (Fe_3C) and austenite -graphite, can nucleate and growth.

Steels and white cast irons obey the metastable iron cementite phase diagram whereas the cast irons obey both the equilibrium iron-graphite and the metastable Fe-Fe_3C phase diagrams. The microstructure of the cast irons, which depends

on the carbon content and solidification rate, must be deduced using both of the phase diagrams. That is why the analysis of structures of cast iron is much more complex than those of the steel and is much more sensitive to the processing conditions, such as molding, melting and casting, pouring, etc. In addition, commercial cast irons are complex alloys that contains appreciable amounts of other elements. The most important addition is silicon ranging from 1.0 to 3 weight % . Thus, it is good to treat cast irons as a ternary alloy of iron, carbon and silicon.

3.- The Iron-Carbon-Silicon

In cast iron, silicon as well as carbon is an important alloying element. The addition of silicon promotes the graphitization in cast iron causing the decomposition of cementite in iron and graphite. The third component Si , changes the eutectic and eutectoid from a univariant reaction at a constant temperature to a univariant reaction occurring over a range of temperatures.[3] The vertical section of the ternary diagram Fe-C-Si is presented in the Figure # A3, in which it is possible to observe the progressive rise in the eutectoid temperature with the increasing silicon content, and the displacement of the eutectoid composition to a lower carbon content.[4] In the same way the eutectic reaction is reduced from 4.25 to 3.65 wt % C with the 2 wt % silicon content in the casting. As consequence of the high carbon content and silicon addition, cast iron contains carbon in

free form as graphite and combined form as cementite, whereas steels only contains carbon in combined form.

4.- The Iron-Carbon-Phosphorous system

Phosphorous is commonly present in cast iron. A small quantity up to 0.1 wt % is soluble in α iron, but larger quantities form the micro-constituent steadite. This complex eutectic of iron and iron phosphide (Fe-Fe_3P) is the last constituent in solidify at the cell boundaries.[5] The iron phosphide is hard and brittle. A microstructure of a casting with a 0.2 wt % P in gray iron shows steadite only in the junction of three cells and has the shape of concave triangle, but with 0.5 wt % P a complete network of steadite can form around the cell. The term cell is used in the field of cast iron solidification to explain a structure of two interwoven crystals, in which all the graphite flakes are interconnected as is the austenite.

Before the development of higher temperatures for pouring molten iron, high phosphorous content irons were commonly used for increased fluidity, especially for thin sections or castings with a complicated shape.

5.- Other elements.

SULPHUR.- All commercially produced iron and steel contain some sulphur. For a long time, the sulphur content was considered a serious problem, and always was reduced to as low a concentration as possible. Sulphur is not entirely undesirable,and in some type of castings, a minimum content is

required to produce the desired microstructure and properties. The influence of sulphur at small melt concentrations is to allow the graphite to growth at smaller interface undercooling than in a sulphur free alloy.[4]

MANGANESE.- The effect of sulphur must be considered in relation with the manganese content of the iron. Without manganese present in the iron, all the sulphur will combine with iron forming an iron sulphide,FeS, which appears at the grain boundaries during the solidification process, but when sufficient manganese is present, all the sulphur combines with it to form manganese sulphide,MnS, which appears as a randomly distributed particles in the matrix. Manganese in excess of the amount required for MnS formation will tend to promote a pearlitic microstructure and increase the strength and hardness.

6.- Solidification

In metallurgical materials, solidification is the transformation process from liquid to solid phases. When a pure liquid solidify, the growth of the solid phase only involves the transfer of heat, but when an alloy solidifies both the transfer of heat and the diffusion of matter must be considered.

The kind of iron which is formed during solidification depends upon the composition of the iron, the presence of nucleating agents and how rapidly the metal is solidified.

Higher carbon and silicon contents promotes graphitization during solidification. Lower carbon and silicon, and the presence of carbide stabilizing alloy elements, tends to prevent the formation of graphite by causing the carbon to remain combined with the iron as iron carbide (Fe_3C) and solidify as white iron.

The structure of all metals is affected by the rate at which they solidify. The usual effect of more rapid solidification is a finer grain size. Thinner section iron castings which solidify more rapidly do have a finer microstructure than the same iron cast into a heavier section. However, more rapid cooling and solidification of cast iron completely change its structure as described in the subsequent sections.

7.- Nucleation

Ideally, as a liquid metal is cooled it should transform to solid as soon as it reaches the freezing temperature. But it does not occur because a formed embryo (nucleus), an atom arrangement in the liquid with the same structure as the solid, is redissolved in the liquid because the additional surface energy of the small particle of solid makes the total free energy of the system greater than the corresponding mass of liquid. When the liquid phase is undercooled, the bulk of small solid formed has a lower free energy than the corresponding mass of liquid, the surface energy of the small particle of solid will not raise the total free energy above

that of the liquid, being a stable particle of solid called nucleus.[3] If a liquid metal is undercooled by several degrees in temperature, ΔT below the melting point (Tm), before it solidifies, solidification will be accompanied by a decrease in free energy, ΔG. This free energy decrease provides the driving force for the solidification process.[6]

7.1.- Homogeneous and heterogeneous nucleation

The initial stage of separation of one solid from the liquid takes place by nucleation, after that the nucleus with the critical dimensions has the chance of growth.

The direct aggregation of atoms in the liquid in the crystallographic order to achieve the critical dimensions is called homogeneous nucleation. The formation of the nucleus creates a new surface between the solid and the liquid , and the well known Gibbs free energy applied to nucleation results in the critical free energy, ΔG^*, and the critical radius, r^*.[6]

However, when the attachment of atoms occur with the aid of some existing surface, it is called the heterogeneous nucleation. In practice, the nucleation in liquids under normal conditions takes place by heterogeneous nucleation. The new solid phase grows either at a mold surface or on a surface of a cluster within the melt. A mathematical model for heterogeneous nucleation considers a spherical segment of a liquid on a flat surface in which the solid, beta, is formed from the liquid, alpha, on the flat substrate.

8.- Interface Stability

In pure metals, solidification is controlled by the rate at which the latent heat of solidification can be conducted away from the solid liquid interface. When a solid grows into a superheated liquid, a planar solid-liquid interface is stable. Consider an interface with small protrusion, and due to the increase of temperature in front of the interface, the protrusion is immediately dissolved, and only a planar solid-liquid interface is possible. On the contrary, if the liquid is supercooled as consequence of the heat transfer process from the liquid, a decreasing temperature from the solid-liquid interface to the liquid is produced, and the tip of the imaginary protrusion achieves a preferential growth condition, where the dendritic growth mode is stable.

9.- The Phase Growth Rate

The growth rate of a phase is dependent on the mechanism which controls the rate of atom attachment to the surface . The controlling mechanism can be diffusion, in which the flux of atoms reaching the surface being incorporated is dependent on the diffusion rate. Alternatively the structure of the interface determines the rate at which atoms are accepted from the diffusion flux. Two type of phases will be considered : (1) metallic phase and (2) non-metallic phases.

The metallic phase which crystallizes from the melt and is of importance in cast iron is austenite (the gamma phase). The gamma phase must growth at a rate determined by solute

diffusion in a liquid.

Graphite is a typically non-metallic phase. It is a faceted crystal and is bounded by crystallographic planes of low index. At small undercooling, its growth is apparently determined by the presence of steps of defect structure at the interface between the bounding crystal faces and the liquid.

In the development of the cast iron, solidification of the gamma-graphite eutectic is of special interest since the structure is determined by two phases growing by different mechanisms.

10.- The Graphite Phase

The graphite phase is a faceted crystal bounded by low index plane as shown in the Figure # A4. In graphite flakes crystallized from liquid iron carbon alloy, the normally bounded planes are (0001) and the {1010} . In the eutectic, the edges of the plate like graphite crystals are not well defined. Unstable growth occurs in such a way that these crystals may be bounded by faces of different orientation. The rate of growth of the faceted graphite crystals is determined by the manner in which the structure incorporates the atoms into the surface.

The Figure # A5, shows a model of two dimensional crystal as a function of the index of the face, the [01] face is smooth, while the [11] and [13] faces have stepped structure, in which the faces [11] and [13] must advance in the direction

normal to their planes by adding atoms on the steps as shown in Figure # A5b, until the surfaces have finally grown out of the crystal, which is then bounded by the low index faces [01].

11.- Growth of Graphite

The growth of a crystal can occurs by two mechanisms: growth from steps due to defects, and growth by nucleation of new faces. In the growth of the crystal by the movement of the steps is indicated in the Figure # A6, in which the atoms attach to defects normally present in crystals such as the screw dislocation, the atoms attach to the step of the spiral and the rotation which results gives a growth of one step high per revolution. At small undercooling, this is the mechanism suggested for the growth (0001) face of graphite.[4]

Another step defect growth mechanism is indicated in the Figure # A7, and is in the form of rotation boundary. The two parts of the crystal are in rotation by an angle ϕ, which has fixed values. The growth of the (1010) faces correspond to this mechanism. The faces would require individual nucleation process for each growth plane and the presence of twining provides a step for the nucleation of the new face.

11.1.- Lamellae Form of Graphite

The rate of growth of the (1010) graphite surface at small undercooling have the form of the Figure # A8, where the growth rate, R, dependence on ΔT is parabolic, $R \alpha \Delta T^2$. At higher undercooling the growth rate is linear, i.e.

$R \alpha \Delta T$.

The rate of growth of the (1010) is indicated as exponential with respect to undercooling, growing edgewise at different values of T depending on the nucleation of the (1010) planes at the step. The curve 1 represents the greatest undercooling for growth if no defect boundary is present. The curve 2 represents the case of low undercooling when the rotation boundary step is present, and the curve 3 represents the minimum undercooling for growth when a contaminating impurity is present (i.e. sulphur) in the melt.

The lamellae form of the graphite is the result of the difference in growth rate between the rotation boundary for (1010) and the growth of the (0001) controlled by the attachment of the steps at the screw dislocations. The ratio of the growth of the two different mechanisms should provide the approximate dimensions of the lamellae graphite which is closed to 10:1 .[4]

12.- Phenomena of Instability in Growth .

For non-metallic materials like graphite, which growth in faceted manner, faces closed to a low index planes have a stepped structure and their growth rate is orientation dependent. As the orientation change, the growth rate should change. Graphite has unusual instability behavior. At small undercooling, branched dendrites from {1010} faces can be noted. This mode of growth stated the radiating structure of the eutectic cell.

The fact that the growth of a metallic dendrites and unstable non-metallic faceted crystals is different, requires a different analytical approach. In the liquid solid interface of metallic solidification it is considered that a protuberance in front of the interface has the chance of growth in constitutional undercooled liquid producing the dendritic growth and developing the arms as a side branch.

In the case of the faceted crystals the instability looks different from the dendritic structure. Also their eutectics do not have the organized geometries of the metallic systems. In faceted crystals, a planar face of has initially a homogeneous supersaturation. As the size of the crystal increases, the supersaturation changes from the center to the corner as shown in the Figure # A9. The different types of growth instabilities which occurs in the graphite are summarized as follows:

(a) Primary crystal branch dendriticaly from faces (1010)
(b) Eutectic crystal branch out of the edge of the lamellae
(c) Steps becomes unstable and form elongated ledges
(d) The ledges becoming unstable grow into the liquid
(e) The ledges can growth round the crystals.
(f) Pyramidal growth can occur on (0001)

13.- Solidification of Cast Iron

In the theory of homogeneous nucleation , the model employed is a spherical nucleus. Since graphite is

anisotropic with different values of interfacial energy on different crystallographic plane, it is considered a disk shape nucleus model of height,h, and radius,r, the edge surface energy has a value ϵ and the flat surfaces of radius r have a surface energy of σ , as indicated in the Figure # A10.

The interfacial free energy, σ, between the nucleated phase and the heterogeneous nucleus has an important influence on the critical free energy for nucleation, as shown in the Figure # A11. The value of σ is dependent on the structure of the nucleus and is related with the coherency of the interface. In a coherent interface, a perfect match between parent and product phases occurs, strains in both sides are involved in which the nucleating substrate is dilated and the nucleating phase is contracted. If the strains are ϵ_1 and ϵ_2 , the total interface strain is $\epsilon = \epsilon_1 + \epsilon_2$

In the semi-coherent interface some parts match perfectly but other regions have a mismatch, and this can be represented by a model of coherent interface with interspace dislocations. The total interfacial energy,σ, is equal to the matching region, σ_c, and the energy of the misfit region, σ_s, and from that $\sigma = \sigma_c + \sigma_s$. A typical example proposed for the semi-coherent interface mismatch is the nucleation of the (0001) hexagonal crystal face on the (111) cube face.

In the incoherent interface, the nucleated phase has no relationship with the parent phase and there is a complete

mismatch between both structures. For the case of nucleation with coherent and incoherent interfaces, the free energy for nucleation is shown in the Figure # A12, for small disregistry, δ, the strain energy term is energetically more favorable so that coherency is preferred, and as δ increases it becomes more favorable to take up the misfit with dislocations, then a semicoherent interface is formed.

In heterogeneous nucleation, it is very important to consider the materials added to the liquid alloy and also the chemistry of the melt. Some of the structural effects related with the heterogeneous nucleation especially considering the alloying elements and impurities are:

(a) The promotion of the graphite crystallization rather than the carbide formation.

(b) Avoidance of the undesirable undercooled structures.

(c) An increase in the frequency of eutectic cell nucleation

14.- Inoculants

Cast irons are usually hypoeutectic in composition and ordinarily would be characterized by the primary growth of the gamma phase. Inoculation prevents the structures dominated by this phase. Most of the commercial inoculants used in cast iron practice consist of Fe-Si, with small amounts of other elements such as Ca, Al, Zr, Ba, Sr, and Ti. The inoculant action is to promote the nucleation of graphite during the eutectic solidification of cast iron, avoiding the formation

of undesirable structures such as ledeburite (eutectic structure of austenite and cementite), which in thin sections tends to dominate.

The eutectic cell number is influenced by inoculation, and the experimental data indicates that the graphite nucleation is mainly by oxides. The silicon dioxide, SiO_2, must form the basis for the graphite nucleation, and other elements of high oxygen affinity are present in the substrate crystal lattice. The nucleation being complex is proposed two stage process, in which the formation of the oxide phase is preceded by the formation of a sulphide. (See next sections)

14.1.- Model of Duplex Sulphide Oxide

Inclusions in graphite extracted from cast iron shown a duplex structure in the nucleus, consisting of sulphide core surrounded by an oxide shell.[4] The nucleus had the following composition:

Core: (Ca,Mg) sulphide

Outer shell: (Mg,Al,Si,Ti) oxide

The orientation relationship in the initial growing complex nucleus and between the oxide phase and graphite were then established :

Nucleus: (110) sulphide parallel to (111) oxide

[110] sulphide parallel to (211) oxide

Nucleus/graphite: (111) oxide parallel to (0001) graphite

[110] oxide parallel to [1010] graphite

15.- The Gamma-Graphite Eutectic

In the Morrogh and Olfield model, illustrated in Figure # A13, it is considered that the graphite is interconnected within the eutectic cell.[7] The idea presented was of a continuous skeleton of graphite which branched with a frequency depending on the radial growth rate of the eutectic cell. Minkoff and Lux[6] added a series of sketches for better understanding of the developing of the eutectic cell, and they say the graphite crystal extends as a thin plate-like from bounded (0001) planes and the branching of the graphite occurs from the side and the branch curves and grows over the parent crystal. The continuous branching of the growing members and

curvature extends the eutectic skeleton in three dimensions, constitutes a behavior reminiscent of the dendritic branching, and also the growing graphite phase is apparent independent of the involved second phase.[6] In addition it could be noticed that this specific behavior of the graphite in the eutectic is due to the assumed stability of the (0001) growth plane and the presence of a rotation boundary defect on (1010).

The interface between the eutectic and the melt appears as non-planar as in the Figure # A14. This apparently is due to the fact that the graphite phase grows by an interface mechanism and requires more undercooling than the γ phase. This results in a non-isothermal process and from that a non-planar interface is produced. It must be noticed that as the eutectic becomes finer, the departure from planarity is reduced as we can see in the Figure # A14b where the interface adjust itself to the temperature conditions. If the austenite and graphite eutectic plates are thick, the graphite grows faster to adjust to the temperature gradient and non-planar interface is produced.

Ahead of the eutectic cell the temperature is also negative originated because the liquid alloy composition undercools by at least 4^0 C, before the graphite nucleates to initiate the eutectic solidification.

In hypoeutectic (regular case) cast iron, the γ phase grows first and the solid separated from the liquid until the later reach the composition and temperature where the graphite

can nucleate. The interdendritic liquid is undercooled and eutectic grow occurs filling the interdendritic spaces between gamma dendrites.

16.- Coarsening Effect by Sulphur

The test results for the lamellae space-growth rate (λ-R) relationship as a function of the sulphur content are shown in the Figure # A15, where for a fixed value of growth rate the λ value increases as sulphur increase until a peak is reached and then once more decrease as the sulphur content increases.[8]

16.1.- The Fineness of the Structure

For a given composition, the undercooling for nucleation of eutectic cell determines the growth rate and hence the fineness of the structure. The greater the undercooling the finer the graphite formed. The second factor is the chemical composition, specially sulphur because the coarseness of the eutectic increases as the sulphur content increases by reducing the growth rate at a given undercooling. It is appropriate to consider that the influence of melt composition in cast iron is to change the interface temperature at a given growth rate. The influence of sulphur at small melt concentrations is to allow the graphite phase growth at smaller interface undercooling than sulphur free alloy. The graphite branching is dependent on the undercooling, then the direct effect results in the coarsening of graphite.

16.2.- Change from coarse to fine structure

As the growth rate increases the value of the

interlamellar space decreases but at a certain point the λ value changes to a second branch of the λ-R curve located at lower λ values.[7] This means that there are a abrupt change from coarse to fine structure at certain growth rate, and both structures can coexist . This is shown in the Figure # A15, where it is possible observe that at a given sulphur content (e.g. 0.022 wt% S) for a growth rate R of $2x10^{-4}$ cm/sec., two lamellae spacing appears,the coarse λ_1 , and the finer λ_2.

17.- The asymmetric zone

In metallic systems, the eutectic coupled zones are uniformly situated between the two liquidus prolongation lines, while in the graphite-iron system it is asymmetric as a consequence of the temperature dependence of growth of the metallic and non-metallic (faceted) phases as shown in the Figure # A16.

In the Figure # A17a, is shown two growth rate curves , in which one of the phases (α) has a marked temperature dependence on the growth rate as for a non-metallic phase (e.g. graphite). It is important to notice that the eutectic structure (two phase structure) lie between the curves for the growth rates of the metallic and non-metallic phases. This gives three regions undercooling dependent, as shown in the Figure # A17b, in the first region primary alpha grows faster than the eutectic, in the intermediate region the eutectic is preferred and in the third region again a single phase grow is produced.

18.- Gray and White Casting Solidification

From practical experience, it is well known that a cast iron melt could solidify as a gray iron by slow cooling and white by rapid cooling. This observation has lead to the idea that each cast iron has a certain critical cooling rate below which it solidifies completely as gray casting and above which it solidifies completely as white casting. Solidification at exactly the critical cooling rate, a mottled structure is formed. This concept of critical cooling rate explain the fact that a casting may have a white casting case and a gray casting core. In the same way, critical cooling rates explain the so called inverse grayness, where white iron shows a gray iron in the surface specially in thin sections.

Figure # A18[7] shows the range of existence of the gray and white structures plotted graphically as temperature versus growth rate. The equilibrium temperature for the iron-graphite eutectic is 1153°C and for the iron-cementite eutectic is 1153°C. Between these temperatures, only the graphite eutectic can nucleate and grow. Below 1148°C the cementite can nucleate and grow. The growth rate of this cementite rapidly exceeds that of the graphite, and at approximately at 1140°C there should be a spontaneous change from gray to white solidification.

Hillert and Rao[7] concluded that:

(1) Graphite is more easily nucleated than cementite,but

(2) Once nucleated, cementite grows faster than graphite.

18.1.- Growth Characteristics of Gray Eutectic

It is a well know fact the graphite flakes in the colony are interconnected such as the austenite dendrites. Consequently it is generally accepted fact that each nucleus of graphite may develop into the eutectic cell in all directions approximately at the same rate (Figure # A19). The result is two interwoven crystals, one of each phase, growing with independent crystal orientation and at different rates. A normal eutectic grows with a high degree of cooperation between phases given a flat eutectic interface, in which a smaller interlamellar spacing, λ, has been established by a branching process.

In the case of gray eutectic it could thus be argued that the branching mechanism is not sufficiently effective to yield the proper number of lamellae to form, given as result a coarse spacing λ as shown in the sketch of the Figure # A19 as the prototype of the graphite eutectic. One should thus conclude that the coarse spacing demonstrated in the Figure # A19 is the characteristic spacing of the graphite eutectic. This observation has lead to the idea that the graphite eutectic does not grow with high degree of cooperation. To probe it, Hiller and Rao [7] made calculations for a cooperative growth of the graphite eutectic and compared with experimentally determined values. The results are shown in the Figure # A20. The correlation was not good and from that Hiller et al. suggested that the cooperative model for the

growth of the graphite is not applicable. The reason for a low degree of cooperation may be that one phase grows faster (separately) than in cooperation with the other phase. As consequence should be considered that graphite is not able to cooperate with austenite in such a perfect way as described in the theory of cooperative eutectic growth.

18.2.- Growth Characteristics of White Cast Iron Eutectic.

The white cast iron solidification can proceed very fast from a single cementite nucleus and spread to all parts of a casting of considerable dimensions. The fast growth of cementite plates is by edgewise growth, and probably by breaking-off of fragments, plates of slightly new orientations are formed successively and the reaction spreads out in a form of a fan.

The austenite in a hypoeutectic cast iron is present in the whole casting before cementite nucleates and start to grow. However,it seems to have no direct effect on the edgewise growth of cementite. In the eutectic reaction, the two phases,cementite and austenite start to solidify in cooperate fashion as shown in the Figure # A21. There is direct evidence that the edgewise growth of cementite is more rapid than the sidewise growth together with austenite, and that cementite is developed as a flat interface. In addition it must be noticed that in presence of a steep temperature gradient during solidification as in small castings, the cementite turns in such a way that the edgewise growth could

take place in the direction of the gradient. The Figure # A22, shows the data for white iron eutectic growth. Here again, the calculations for cooperative growth shows faster growth rates than those experimentally obtained for white casting eutectic, and the model did not apply, but the degree of agreement is better than the case of gray iron eutectic.

18.3.- Gray or White Solidification of Cast Iron

The gray or white solidification mode of cast iron is dependent on the relative nucleation possibility and growth rates of the graphite and cementite phases. This will depend on alloy chemistry of the melt and on the phase growth in the stated conditions.

The first point to notice is the important action of the inoculants to promote the graphite nucleation and growth. Second, the chemical composition especially in relation with the sulphur content because of the coarsening effect during the solidification of the casting, and third growth rate which lead the graphite or cementite dominate during the solidification process.

19.- Structure and Mechanical Properties in Grey Cast Iron

The mechanical properties of cast iron depends on the microstructure, which is obtained as consequence of the chemical composition, solidification behavior, and cooling rate.[9]

To predict quantitatively the solidification of the cast iron is difficult due to its complex growth. The

solidification is dominated by the eutectic growth of austenite and graphite. The graphite can growth in different ways and show different morphologies.

Srinivasan and Kondic[10] have shown that tensile strength and hardness of cast iron of a constant chemical composition, change in function of the solidification rate and the solid state transformations. The interesting point to notice is that with a constant matrix, the tensile strength, hardness and Young's modulus change with different graphite morphologies. In other words, the shape, the size,and distribution of the graphite, as well as the cell size, have a big effect in the mechanical properties of the cast iron.

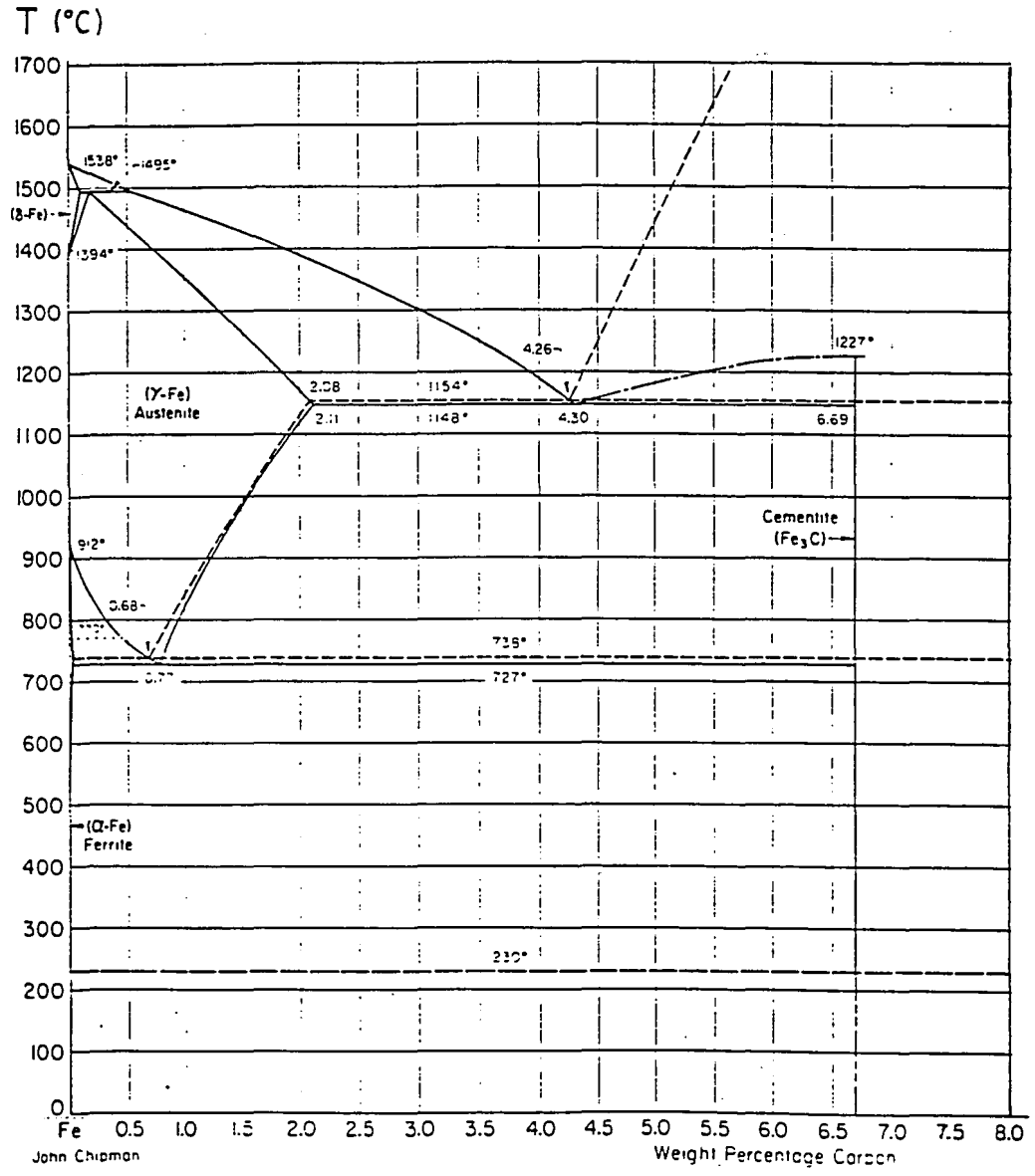

Figure # A1 : Iron-Carbon Phase Diagram[1] . The solid lines correspond the metastable iron-cementite system. The dashed lines, the stable iron-graphite system.

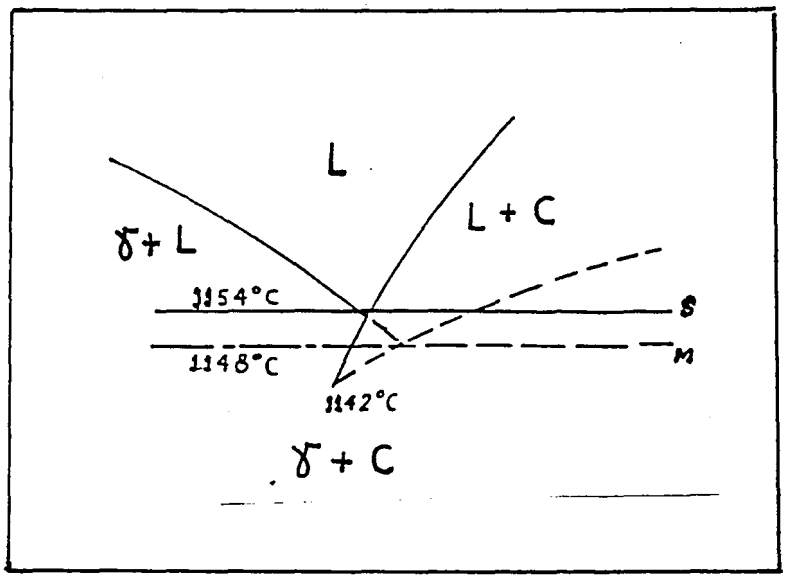

Figure # A2. The eutectic region showing temperatures for the stable and metastable reactions.[2]

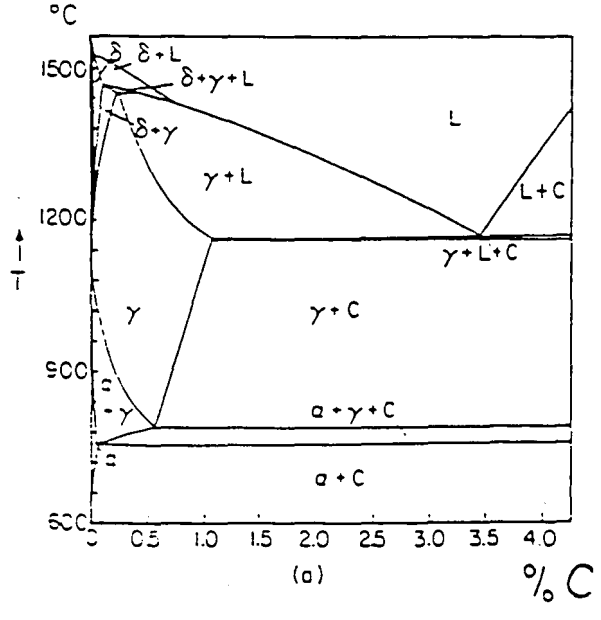

Figure # A3a. Vertical sections of the Fe-C-Si diagram[4]. (a) 2.4% Si.

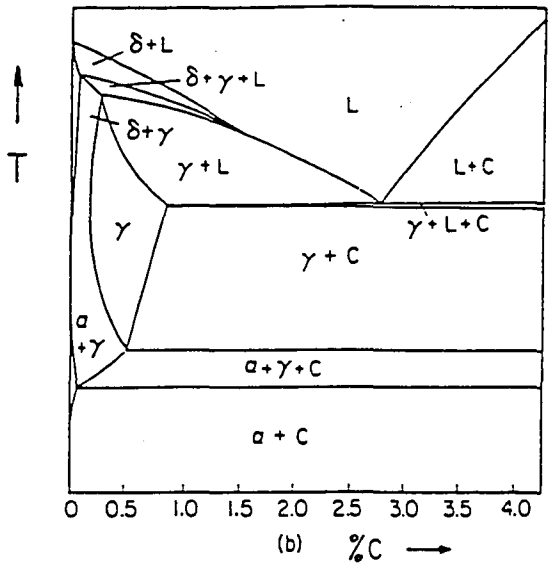

Figure # A3b. Vertical section of the Fe-C-Si diagram.[4] (b) 4.8 % Si.

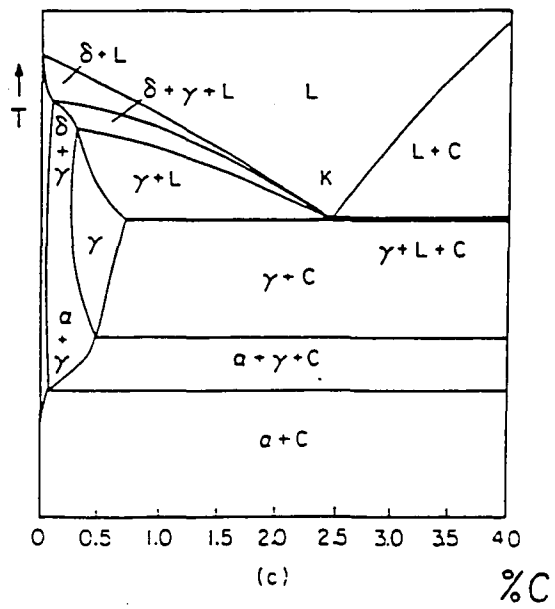

Figure # A3c. Vertical section of the Fe-C-Si diagram.[4] (c) 6.0% Si.

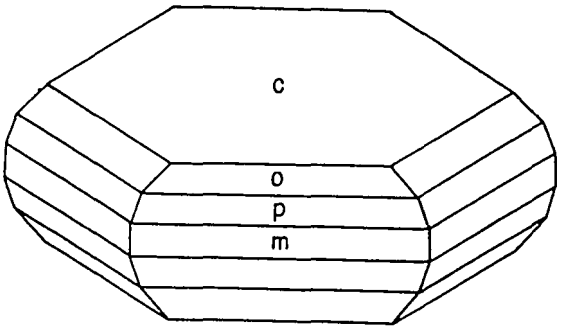

c (0001)
o ($10\bar{1}2$)
p ($10\bar{1}1$)
m ($10\bar{1}0$)

Figure # A4. Facets on a natural crystal of graphite[4]

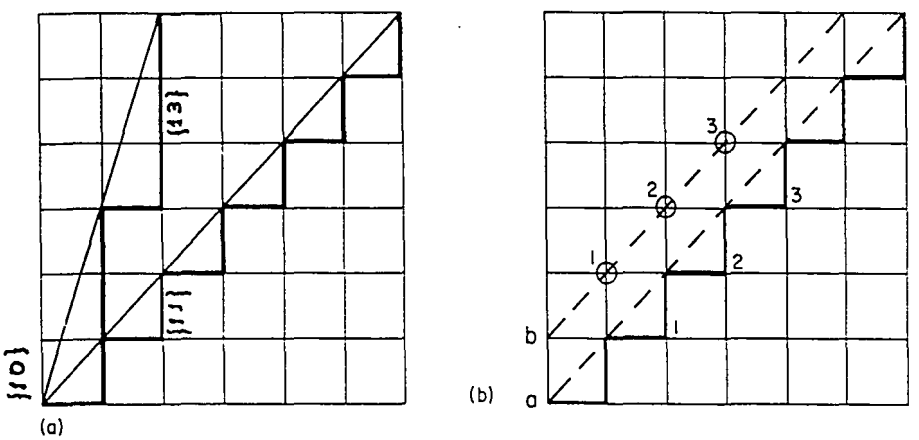

Figure # A5. Stepped structure of two dimensional crystal.[4]

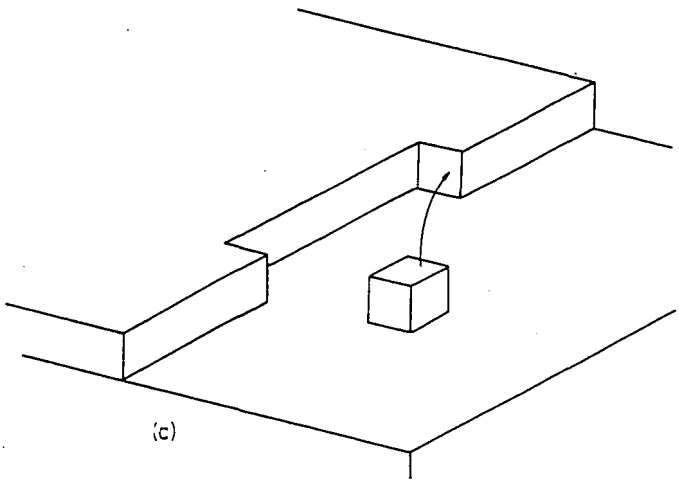

Figure # A6. Growth on a faceted crystal due to atom attachment[6]

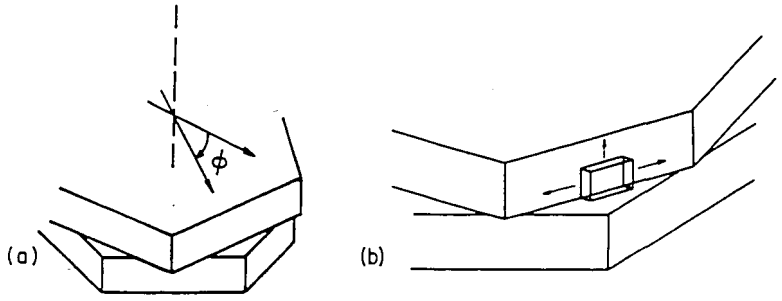

Figure # A7. Step defect in graphite in the form of rotation boundary[6].

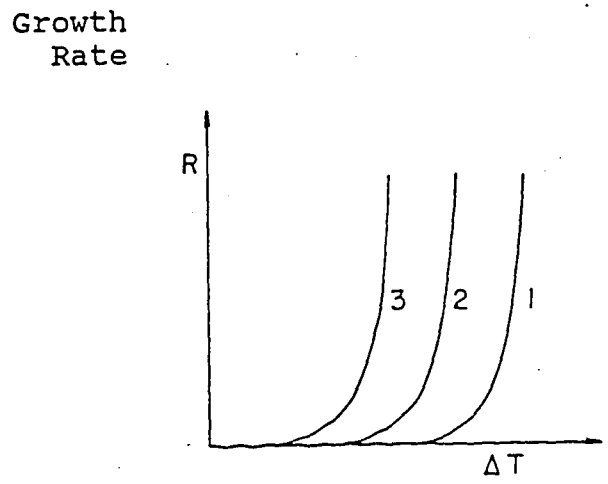

Figure # A8. Growth rate of a (1010) faces is suggested to be nucleation dependent and exponential.[4]

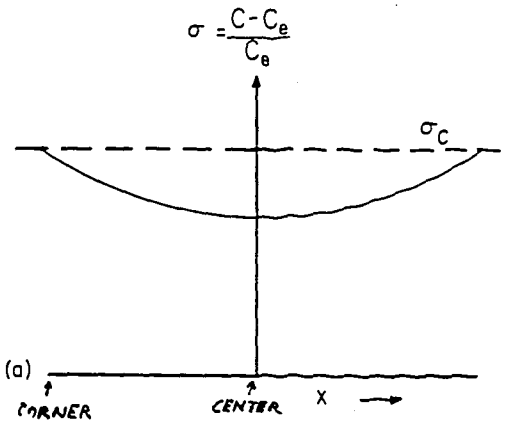

Figure # A9. Curve for the supersaturation, σ,existing over a planar surface. C= solution concentration , Ce = equilibrium concentration, σ_c = critical supersaturation.[4]

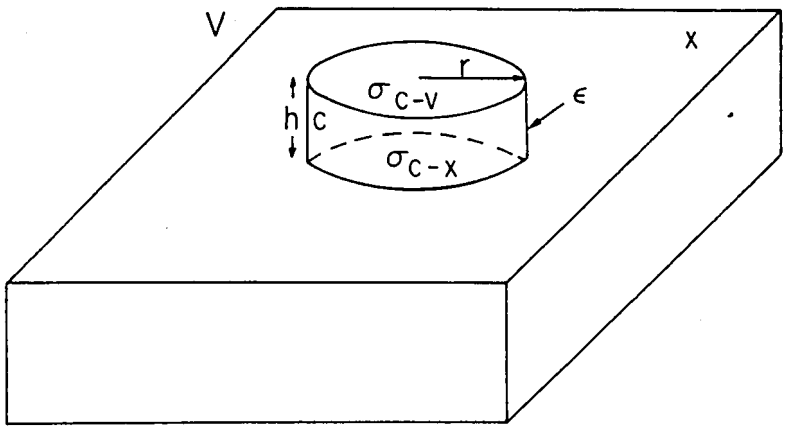

Figure # A10. Disc-shaped nucleus of C phase on a substrate of phase X growing from vapor V. The edge energy is ϵ, σ_{c-v}, σ_{c-x}, are the surface energy.[2]

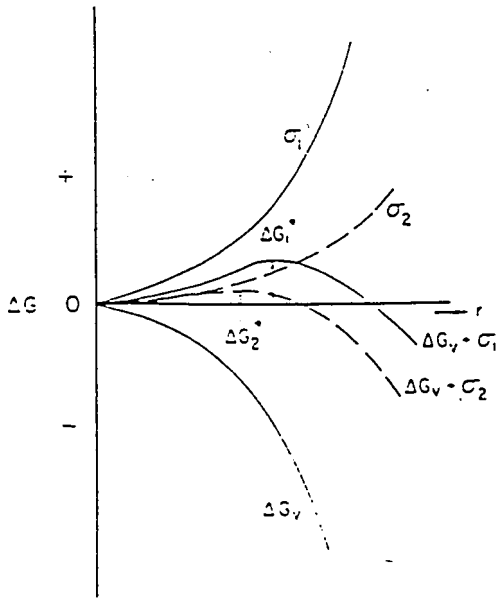

Figure # A11. Free energy change ΔG during nucleation on a substrate. σ_1, and σ_2, are different values of interfacial energy.[4]

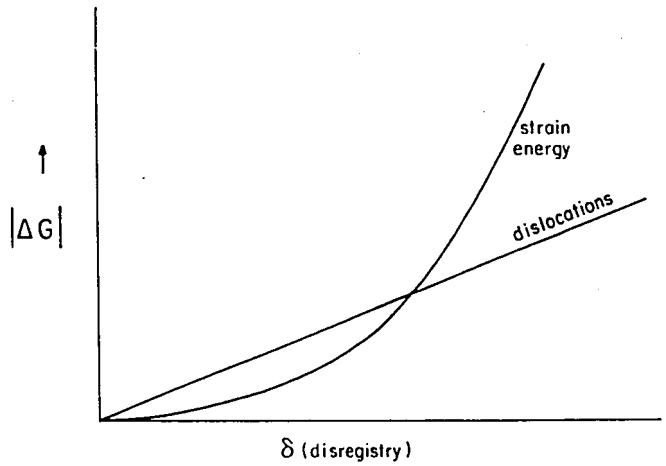

Figure # A12. Free energy for coherent and incoherent interfaces.[4]

Figure # A13. Model of a graphite eutectic cell.[4]

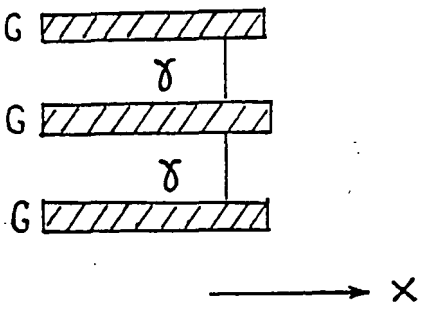

Figure # A14a. Non planar interface of graphite lamellae in eutectic growth[6].

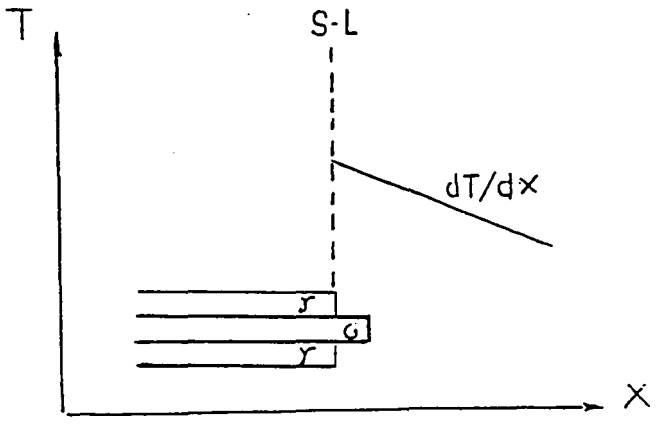

Figure # A14b. Growth of graphite eutectic in negative gradient in front of the interface solid-liquid.[4]

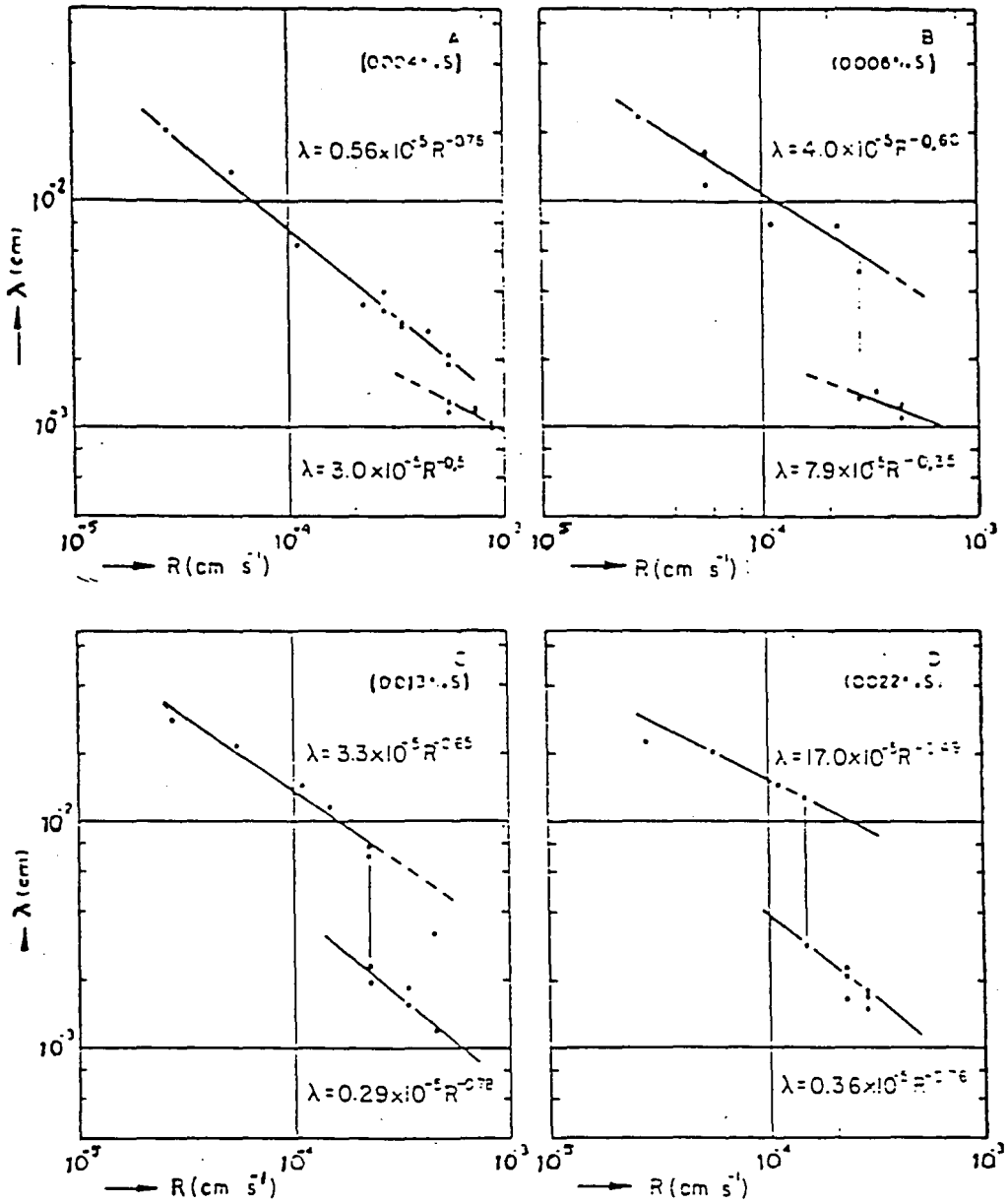

Figure # A15. Relation between lamellae spacing, λ, and growth rate, R, for different sulphur content. At high growth rates the relationship changes to a second curve.
A=0.004% S,B=0.006% S, C= 0.013% S, D= 0.022% S.[8]

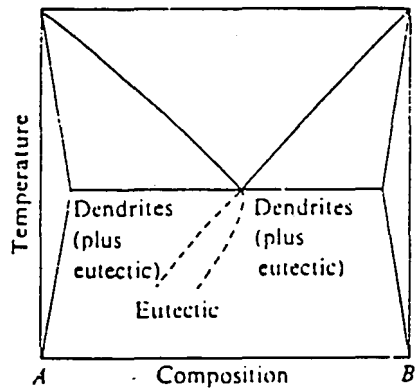

Figure # A16. Diagram of an asymmetrical coupled zone in an eutectic system with one faceted (graphite) phase.[5] A coupled region indicates the extent of a two phase (eutectic) growth region. The graphite-austenite system is asymmetric.

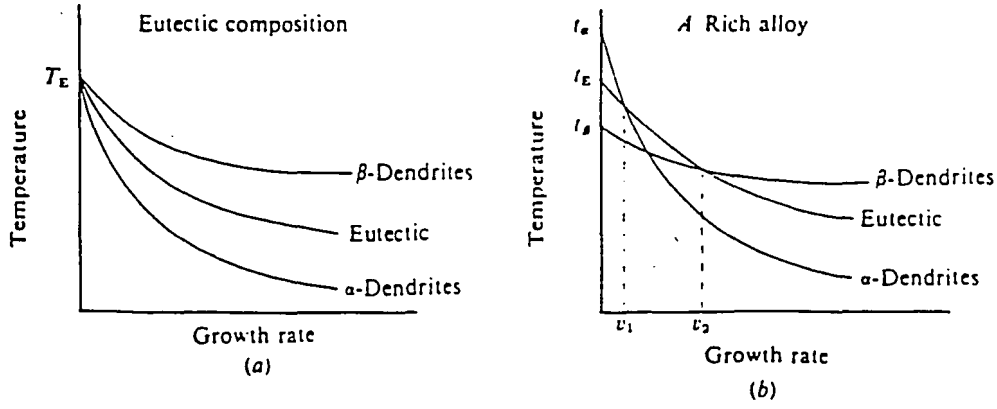

Figure # A17. Growth rate curves of phases α and β, and the α/β eutectic for an asymmetrical coupled region. (a) Eutectic composition. (b) Hypo-eutectic composition[4].

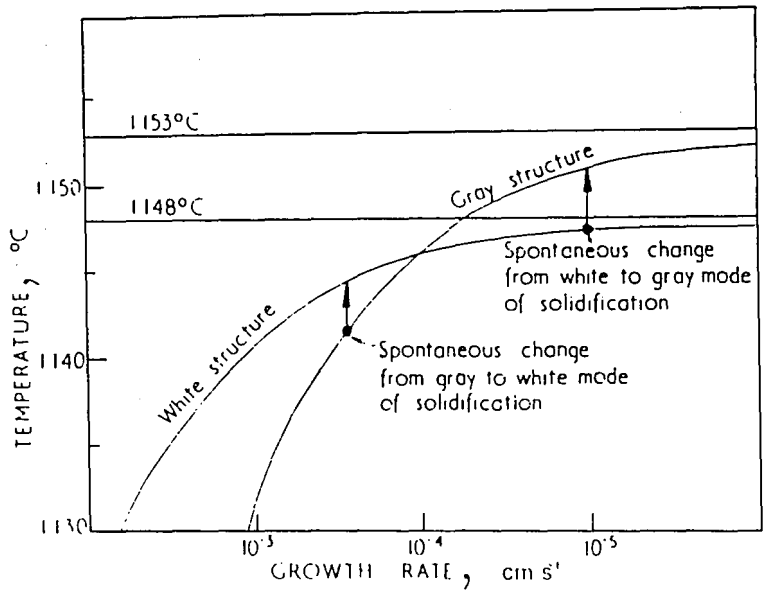

Figure # A18. Range of existence of gray and white cast iron structures.[7] To the right of the intersection (10^{-4}cm/s) the grey structure dominates (lower growth rate), and white structures dominates at the left.

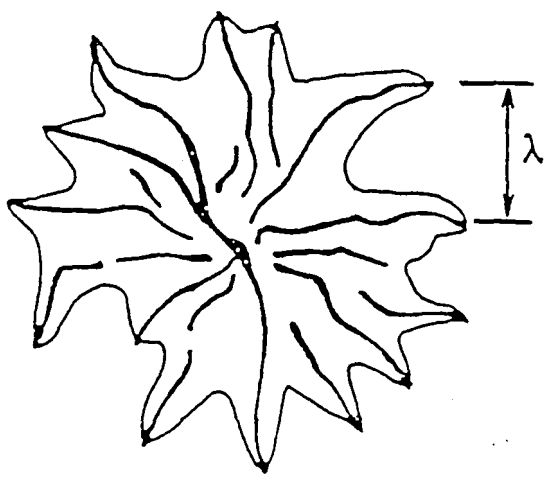

Figure # A19. Shape of gray eutectic cell growing at slow cooling.[7] λ = interlamellar spacing.

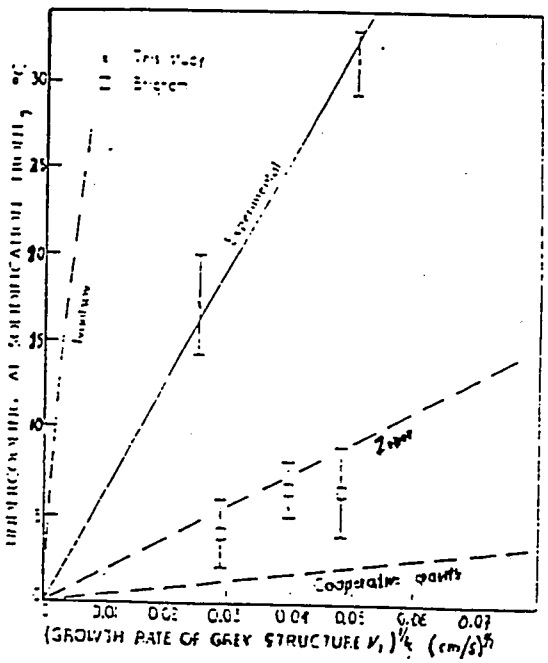

Figure # A20. Theoretical cooperative growth mode of the graphite eutectic compared with experimental values. The correlation is not good, because in the experimentation one of the phases grows faster.[7]

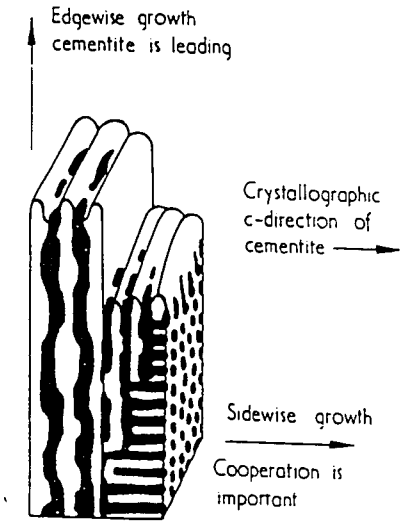

Figure # A21. Formation of eutectic structure in white cast iron. White phase is cementite; black phase is austenite. [7]

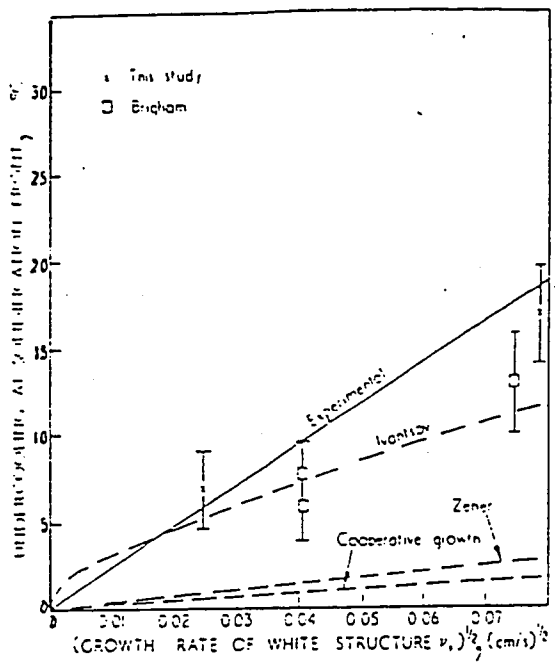

Figure # A22. Cooperative growth mode of white iron eutectic compared with experimental values. The correlation is better than for gray iron. Therefore,white iron growth might be controlled by the growth of the cementite phase.[7]

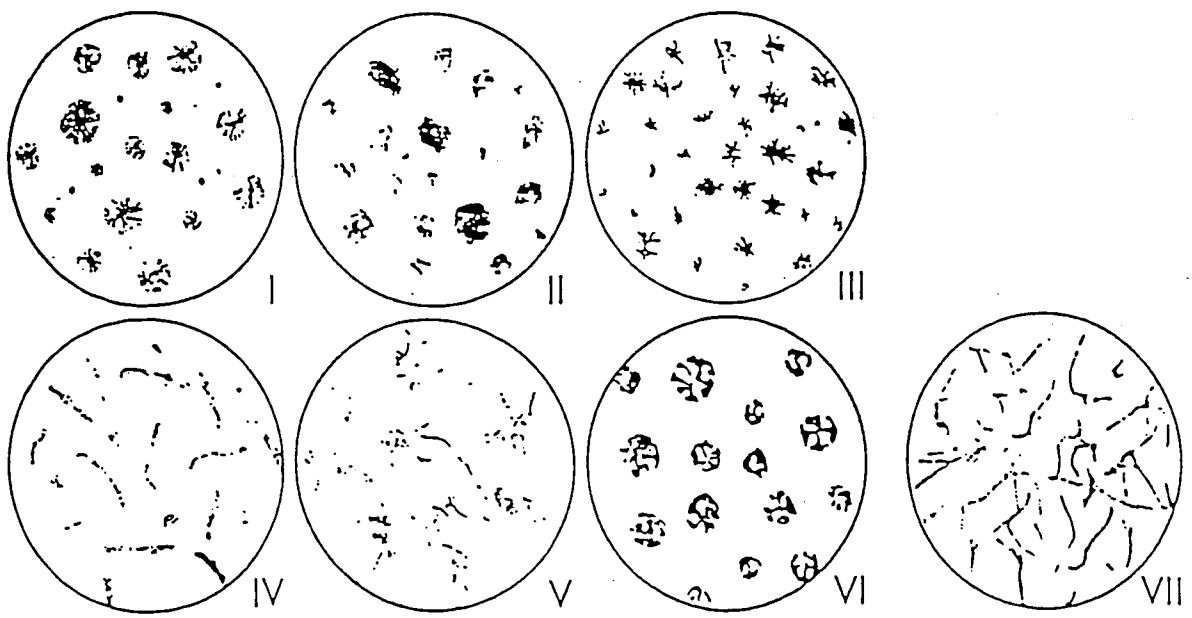

Figure # A23. Graphite type as established by ASTM A-247. [11]

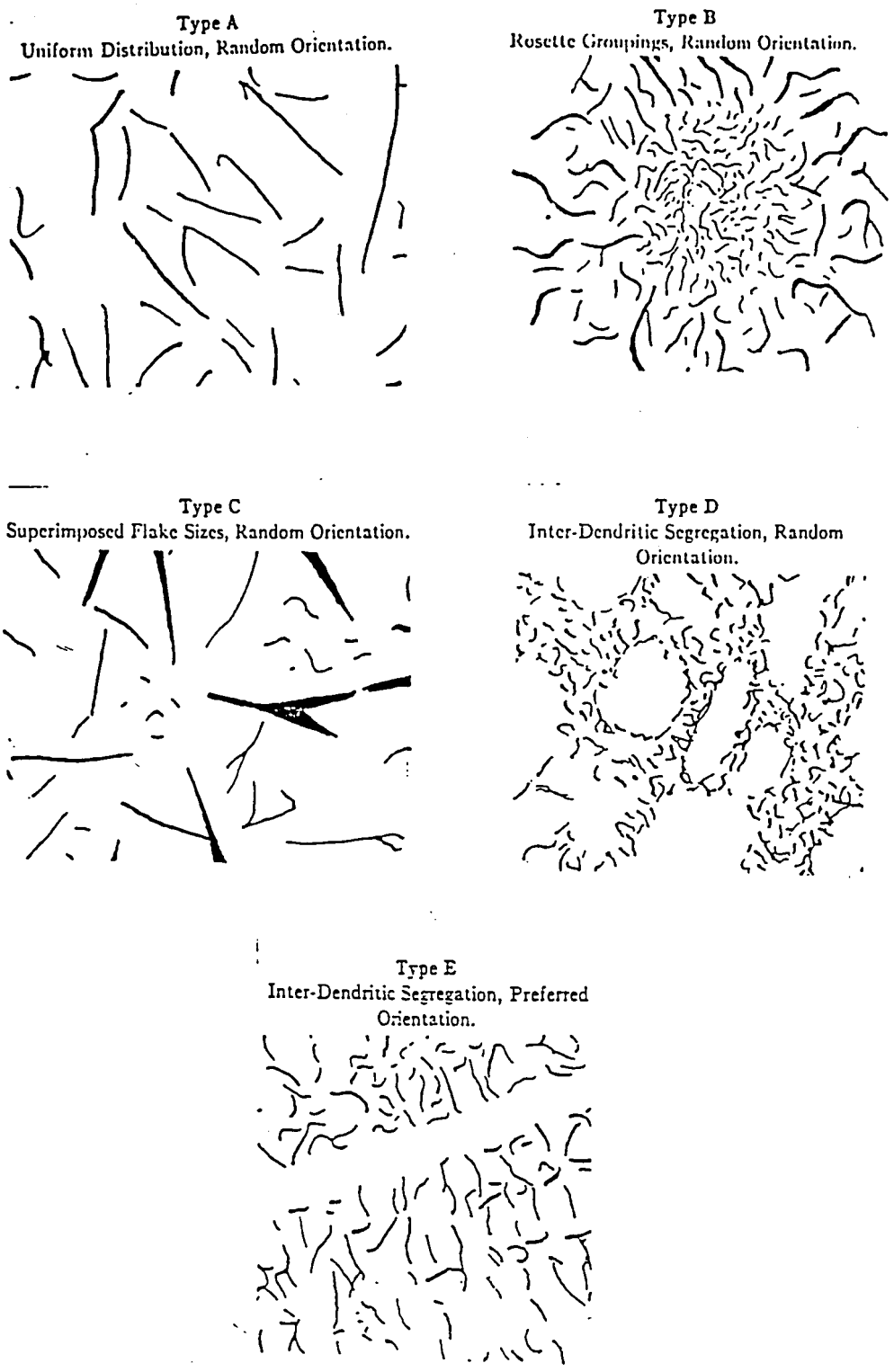

Figure # A24. The five types of flakes of graphite. ASTM A-247. [11]

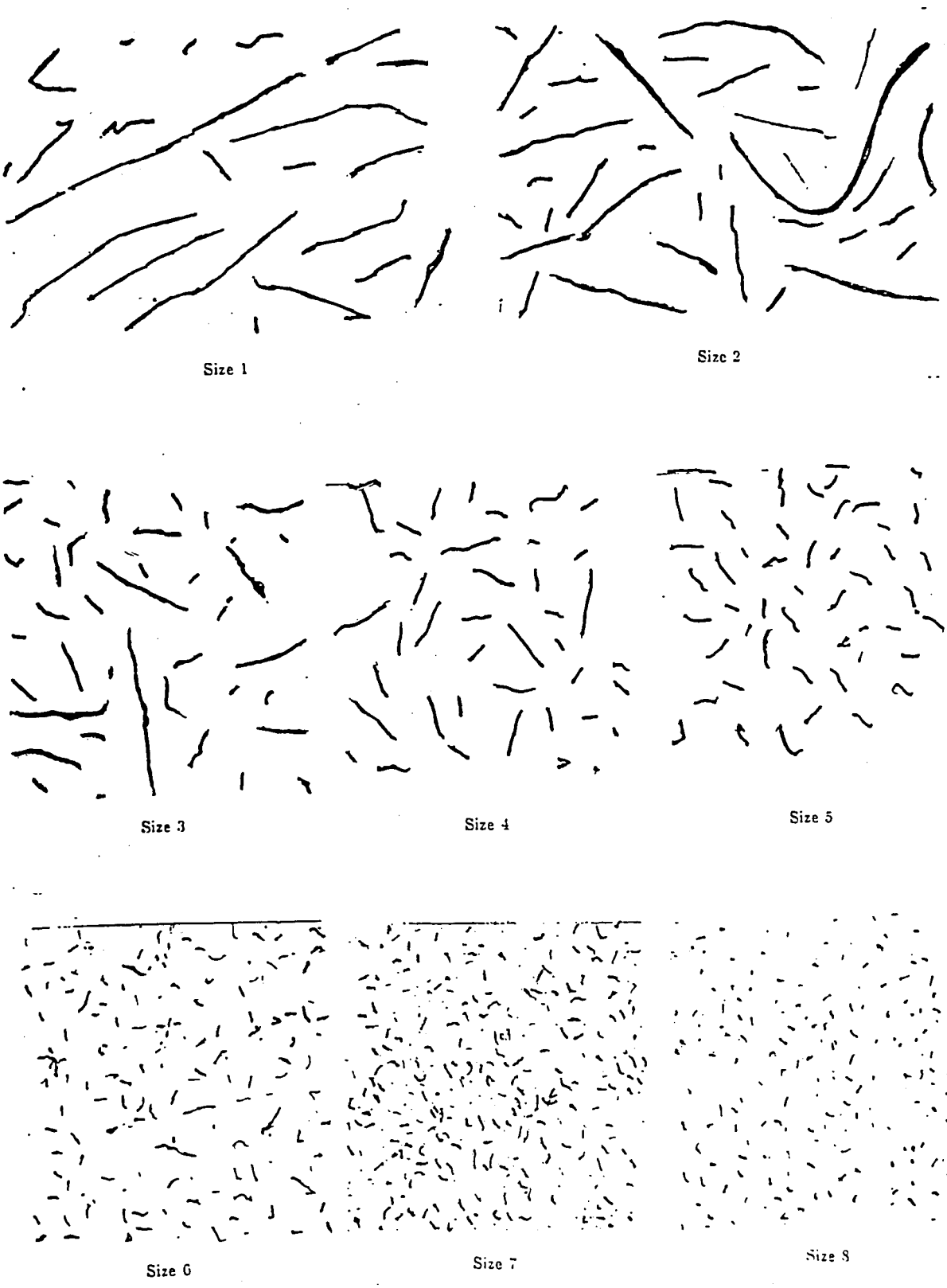

Figure # A25. Flake size chart for ASTM A-247.[11]

REFERENCES:

1.- Metals Handbook, Vol.8,Metallography,Structure and Phase Diagrams, 8th Ed.; A.S.M.;Metals Park, Ohio,1973.

2.- Hillert, M,; Recent Research on Cast Iron; E. Merchant Pub.; New York,1968.

3.- Brick,R.M.;Pense,A. and Gordon,R.B.;Structure and Properties of Engineering Materials; Mc Graw Hill,New York,1977.

4.- Minkoff,I.; The Physical Metallurgy of Cast Iron; John Wiley, New York, 1983.

5.- Walton,C.; Opar,T.; Iron Casting Handbook; Iron and Casting Society, Inc.;1981.

6.- Porter,D.;Easterling,K.; Phase Transformations In Metals and Alloys; Van Nostrand, New York,1981.

7.- Hillert,M.;Suba Rao; The Solidification of Metals; The Iron and Steel Institute-110, London,1968.

8.- Neswagg,H.;Zuthoff,A.; The effect of S,P,Si and Al. on the Morphology and Graphite Structure of Directionally Solidified Cast Iron; Metallurgy of Cast Iron, Georgy Pub.

9.- Lundback,E.; Svensson,I.L.;Thorbrimssom,J.T.; Sodification Processing; The Institute of Metals,1987.

10.- Srinivasan,N. and Kondic,N.; The Metallurgy of Cast Iron; Georgy Pub. Co.;Switzerland,1975.

11.- Standard ASTM A-247; The American Society for Testing and Materials;Philadelphia,Pa; 1990.

12.- Sinha,A.K.; Ferrous Physical Metallurgy, Butherworths, Stone Ham,Mass.,1989.

VITA

Hernan P. Estupinan, was born on May 27,1950 in Quito,Ecuador. He attended the Mejia High School from 1963 to 1969. Upon graduation from high school, he attended the Escuela Politecnica Nacional, in Quito, where he graduated in December of 1977 with a Mechanical Engineer degree.

Hernan enrolled to the staff of Polytechnic National School, Mechanical Engineering College in December of 1977 as Research Assistant, where he later was promoted to different categories until on December of 1984 he became Principal Professor. From 1980 to 1989 he was Head of the Foundry Division of the Metallurgy and Materials Department.

He had been teacher of the following courses: Physical Metallurgy I and II, Engineering Materials I and II, Foundry Technology, Solidification, Welding Principles, and Iron and Steel Transformations.

In 1988 he obtain a Fulbright-Laspau Commission scholarship to pursue his Master Degree in United States of America. In fall of 1989, he entered the graduate program at Lehigh University at the Materials Science and Engineering Department, where he received the Master of Science Degree in 1992.

END

OF

TITLE